



Aerosols from anthropogenic and biogenic sources and their interactions: modeling aerosol formation, optical properties and impacts over the central Amazon Basin

Janaína P. Nascimento¹, Megan M. Bela^{5,6}, Bruno Meller², Alessandro L. Banducci⁸, Luciana V. Rizzo⁷, Angel Liduvino Vara-Vela⁴, Henrique M. J. Barbosa², Helber Gomes^{9,10}, Sameh A. A. Rafee³, Marco A. Franco², Samara Carbone^{11,2}, Glauber G. Cirino¹², Rodrigo A. F. Souza¹, Stuart A. McKeen^{5,6}, and Paulo Artaxo²

¹Post-graduate Program in Climate and Environment (CLIAMB), National Institute for Amazonian Research and Amazonas State University, Manaus, AM, Brazil

²Institute of Physics, University of Sao Paulo, Sao Paulo, SP, Brazil

³Department of Atmospheric Sciences, Institute of Astronomy, Geophysics and Atmospheric Sciences, University of São Paulo, SP, Brazil

⁴Center for Weather Forecasting and Climate Studies, National Institute for Space Research, Cachoeira Paulista, Sao Paulo, SP, Brazil

⁵Cooperative Institute for Research in Environmental Sciences, University of Colorado, Boulder, CO, USA

⁶NOAA Earth System Research Laboratory, Boulder, CO, USA

⁷Department of Environmental Sciences, Institute of Environmental, Chemical and Pharmaceutics Sciences, Federal University of Sao Paulo, Sao Paulo, SP, Brazil

⁸Department of Physics, Colorado State University, Fort Collins, CO, USA

⁹Institute of Atmospheric Sciences, Federal University of Alagoas, Maceió, AL, Brazil

¹⁰Department of Meteorology, Federal University of Campina Grande, Campina Grande, Brazil, PB, Brazil

¹¹Federal University of Uberlândia, Uberlândia, MG, Brazil

¹²Department of Meteorology, Geosciences Institute, Federal University of Pará, PA, Brazil

Correspondence: J. M. P. Nascimento (janaina@if.usp.br)

Abstract.

The Green Ocean Amazon experiment - GoAmazon2014/5 explored the interactions between natural biogenic forest emissions from Central Amazonia and urban air pollution from Manaus. Previous GoAmazon2014/5 studies showed that nitrogen oxides ($\text{NO}_x = \text{NO} + \text{NO}_2$) and sulfur oxides (SO_x) emissions from Manaus strongly interact with biogenic volatile organic compounds (BVOCs), affecting secondary organic aerosol (SOA) formation. In previous studies, ground based and aircraft measurements provided evidence of SOA formation and strong changes in aerosol composition and properties. Aerosol optical properties also evolve, and their impacts on the Amazonian ecosystem can be significant. As particles age, some processes such as SOA production, black carbon (BC) deposition, particle growth, and the BC lensing effect change the aerosol optical properties, affecting the solar radiation flux at the surface. This study analyzes data and models SOA formation using the Weather Research and Forecasting with Chemistry (WRF-Chem) model to assess the spatial variability of aerosol optical properties as the Manaus plumes interact with the natural atmosphere. The following aerosol optical properties are investigated: single scattering albedo (SSA), asymmetry parameter (g_{aer}), absorption Ångström exponent (AAE), and scattering Ångström exponent



(SAE). These simulations were validated using ground based measurements at three experimental sites: Amazon Tall Tower Observatory - ATTO (T0a), downtown Manaus (T1), Tiwa Hotel (T2) and Manacapuru (T3), as well as the G1 aircraft flights. WRF-Chem simulations were performed over seven days during March 2014. Results show a mean biogenic SOA (BSOA) mass enrichment of 512% at the T1 site, 450% in regions downwind of Manaus such as the T3 site and 850% in areas north of the T3 site in simulations with anthropogenic emissions. The SOA formation is rather fast, with about 80% of the SOA mass produced in 3-4 hours. Comparing the plume from simulations with and without anthropogenic emissions, SSA shows a downwind reduction of approximately 10%, 11% and 6% at the T1, T2 and T3 sites, respectively. Other regions, such as those further downwind of the T3 site, are also affected. G_{aer} values increased from 0.62 to 0.74 at the T1 site and from 0.67 to 0.72 at the T3 site when anthropogenic emissions are active. During the Manaus plume aging process, a plume tracking analysis shows an increase in SSA from 0.91 close to Manaus to 0.98 160 km downwind of Manaus as a result of SOA production and BC deposition.

1 Introduction

Aerosol particles are present in the atmosphere in highly variable types and concentrations, which contribute differently to climate forcing, cloud formation and development, as well as ecosystem impacts. Particles may have a cooling or heating effect on the atmosphere, and their climatic roles are defined by their interactions with solar and terrestrial radiation fluxes, which strongly depend on their optical properties (extinction coefficient, SSA, g_{aer} , etc.). Radiation attenuation by atmospheric constituents is described by the radiative transfer equation, which requires information on the intensive and extensive optical properties of particulates and gases (Boucher, 2015). The aerosol's effect on radiation can be direct, semi-direct, or indirect. Direct effects are related to scattering and absorption of solar radiation by aerosol particles. These effects tend to dominate under clear sky conditions. Indirect effects involve the aerosol influence on cloud formation and development through cloud droplet activation via cloud condensation nuclei (CCN) (Haywood and Boucher, 2000).

Recent studies in Amazonia that integrated data from ground-based sensors (e.g., Martin et al., 2016; Rizzo et al., 2013; Andreae et al., 2015; Artaxo et al., 2013) with regional numerical simulations (e.g., Rafee et al., 2017; Shrivastava et al., 2019; Medeiros et al., 2017) advanced our understanding of the interactions in Amazonia background aerosol urban anthropogenic emissions. However, none of these studies have quantified the impact of atmospheric aerosols on the Amazonian radiative forcing.

A previous study conducted over the Amazonian region during the GoAmazon2014/5 experiment found strong SOA production, with an enhancement of BSOA formation in both the Manaus plume and its outflow by a factor of 100–400% on average during the afternoon of March 13, 2014 (Shrivastava et al., 2019). In Southeast Manaus, de Sá et al. (2018) showed an increase in SOA ranging from 25% to 200% under polluted conditions compared to background conditions, including contributions from both primary and secondary particulate matter (PM). All of these studies are related to an idea suggested in Palm et al. (2018), that anthropogenic emissions play a significant role in SOA production. Cirino et al. (2018) indicate that during the dry season an increase of 40% in the mass concentration of organic aerosols is attributed to SOA formation during



transport from Manaus to downwind sites (T2 and T3). Conversely, the same increase was not observed during wet season. The Manaus anthropogenic emissions are rather constant over the year, representing the major influence on the anthropogenic organic aerosol source and contributing to the OA increase downwind of Manaus (de Sá et al., 2018; Shrivastava et al., 2019; Martin et al., 2010).

50 A possible strategy to improve estimates of the urban plume impact on optical properties downwind of Manaus is to create modeling regional scenarios with and without anthropogenic emissions, and comparing them to analyze how the emissions affect aerosol properties. Other studies have used sensitivity scenarios to understand how aerosol optical properties and secondary formation can be affected by events such as biomass burning (Vara-Vela et al., 2018) or urban pollution (Shrivastava et al., 2019). Many studies have focused on improving the understanding of an urban plume's impact on aerosol optical prop-
55 erties by comparing measurements during background conditions with periods affected by the pollution plume (Palacios et al., 2020; de Sá et al., 2019; Brito et al., 2014; Rizzo et al., 2013, 2011). However, little work has been done to analyze the atmospheric chemistry in the regions typically within the plume but without the plume's effects. This is particularly critical during the wet season, when aerosol levels associated with biomass burning are low and biogenic aerosols become more sensitive to external disturbance. Numerical simulations with high-resolution regional models such as the Weather Research and Forecast-
60 ing Model with Chemistry (WRF-Chem; Grell et al. (2005)) are necessary for this strategy to quantify the effects of urban areas on aerosol levels and ultimately on the ecosystem, especially in regions that lack ground based observations.

Different aerosol optical properties have been used to study aerosol impacts on ecosystems and the radiation balance, such as SSA (e.g., Dubovik and King, 2000; Lim et al., 2014; Russell et al., 2010; Rizzo et al., 2013), SAE and AAE (e.g., Romano et al., 2019; Palacios et al., 2020), and g_{aer} (Korras-Carraca et al., 2015). The significant impacts of Manaus urban
65 emissions on the characteristics of the aerosol population (size distribution, quantity, chemical and physical composition) in regions downwind of Manaus have been described by Rizzo et al. (2013). However, there are no results considering simulation scenarios when the Manaus pollution plume component is turned on and off.

The objective of this work is to model secondary aerosol formation in Central Amazonia, comparing modeled scenarios with and without anthropogenic emissions, examining the interactions between natural biogenic emissions urban air pollution from
70 Manaus and investigating their impact on aerosol optical properties. We have extensively validated the model predictions with ground-based measurements, and estimate how the optical properties may be affected by the plume aging process (see Fig. 1a). This is the first study to our knowledge that focuses on aerosol optical properties such as SSA, g_{aer} , and absorption and scattering coefficients over a geographically extended area over Central Amazonia, using numerical simulations and ground based data.

75 2 Model Description, Emissions and Observations

2.1 Study Region and Methodology

The Amazonian region has an annual mean temperature of around 26°C due the intense solar radiation reaching the surface (Nobre et al., 2009), with an annual average precipitation of 2,300 mm year⁻¹ (Fisch et al., 1998). In the wet season (between

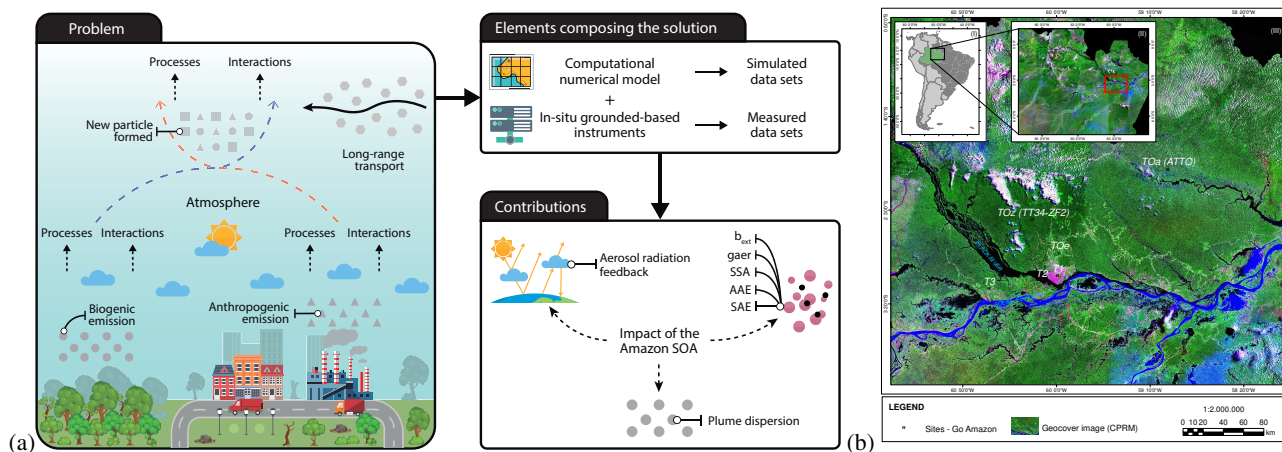


Figure 1. (a) Problem: The atmosphere with different pollution and natural sources and the interactions between them. Elements composing the solution: Computational numerical model and observational data sets. Contributions: Understanding the impact of the Manaus air pollution plume on aerosol optical property variability over the Amazon rainforest during the GoAmazon2014/5 experiment. (b) Sampling stations TT34-ZF2 (T0z) (ca. 60 km northwest) and ATTO (T0a) (ca. 150 km northeast), are both upwind of Manaus; Downtown Manaus (T1), Tiwa Hotel (T2) (ca. 8 km direction) and Manacapuru (T3) (ca. 70 km direction), are all downwind of Manaus. (I) South America and Brazil map. (II) Amazon region, the red rectangle indicates the area where the GoAmazon2014/5 experiment meteorology stations were located and the region used for the WRF-Chem simulations.

January and May), with the Inter-tropical Convergence Zone (ITCZ) extending south over Manaus, it is possible to find one of the lowest particle number concentrations over a continental area in the world (Andreae et al., 2015; Artaxo et al., 1994; Martin et al., 2016). In the wet season, the very high precipitation rate makes it virtually impossible for fires to occur, so the atmosphere is dominated by biogenic emissions, with an episodic component of Sahara desert dust and biomass burning emissions transported from Africa (Artaxo et al., 1990, 1993, 2013; Pöhlker et al., 2018, 2019)

Manaus is a city located in central Amazonia at latitude $3^{\circ}06'07''$ and longitude $60^{\circ}01'30''$. It currently has a population of about 1.8 million and an urban area of 377 km^2 . For this study we focus on a region centered on Manaus extending from latitudes -5.3° S to -0.76° S and longitudes -63.07° W to -56.90° W (see Fig. 1b). This 600 km by 450 km approximately rectangular area comprises the urban area of Manaus, its satellite cities and the surrounding Amazonian forests.

Our WRF-Chem simulation was performed over seven days between 7 and 14 March 2014. This period is part of the wet season in the region (Fisch et al., 1998; Martin et al., 2017). The first day were used as a spin-up period, as such they are discarded from any analysis. Corrections based on the methodology used in Cosgrove et al. (2003) were applied to the simulated temperature values aiming for better agreement between the topography height represented by the model and the one from the GoAmazon2014/5 experiment site.

The choice of the simulated days was made based upon ground-based data availability, which is necessary to evaluate the performance of the model, and the suggestions of Shilling et al. (2018), Shrivastava et al. (2019) and Martin et al. (2017) which



95 highlight the March 13, 2014 as a golden day to study the evolution of the Manaus plume as it advected to the surrounding Amazon tropical forest. Our investigation focuses on a detailed analysis of March 13, 2014, because on that day the plume reached regions downwind of Manaus such as the T2 and T3 sites. During this period mostly sunny skies were observed with little or no precipitation and the interference from biomass burning and cloud processing was negligible. We track the simulated Manaus plume as it ages in order to investigate the evolution of optical properties. Different analyses of atmospheric variables with and without anthropogenic emissions were used to characterize changes in aerosol properties downwind of Manaus due to anthropogenic activity.

To track the plume as it ages, its approximate location and extent over time were determined using the Hybrid Single-Particle Lagrangian Integrated Trajectory (HYSPPLIT) model (Draxler, 2007; Stein et al., 2007). Forward trajectories were calculated starting from 8 points at 200 masl in a circle of radius 0.03° (~ 3.4 km) centered on the plume's initial location at 6:00 LT. Winds and other forcing meteorological fields were taken from our WRF-Chem simulation. Average gas and aerosol concentrations and optical properties were calculated in the volume defined by the maximum and minimum latitude and longitude of the 8 points, and altitude range from 100 to 500m. The averaging region is shown in Figure S12 in the SI, and the altitude of the plume is shown in Figure S14 and S15 in the SI. ΔCO was determined by taking the difference in carbon monoxide (CO) between simulations with anthropogenic emissions turned on and off in the simulated region selected by HYSPPLIT. The tracking plume approach was used to track the plume in other days (10 to 14 March 2014) in order to investigate the change in SOA formation due to different NO_x concentrations. The days other than the 13th were not exemplary days for observing the evolution of the Manaus plume due to meteorological factors such as precipitation. Additionally, the plume did not appear until 8 LT. As such, our analysis focuses on March 13, 2014.

2.2 WRF-Chem Model Description and Setup

115 The study region was simulated with the WRF-Chem regional model, version 3.9.1.1 (Grell et al., 2005; Fast et al., 2006) using full coupled and online meteorology, gas-phase chemistry and aerosol feedback. The model grid covered the study region with a horizontal grid spacing of 3 km and $n_x = 200$ and $n_y = 150$ grid points. Vertically, hybrid sigma coordinates were used to split the atmosphere into 51 levels, the bottom 10 within the planetary boundary layer (PBL). Data from the Global Model Data Assimilation System (GDAS), with a horizontal grid spacing of 1° and 26 vertical levels was used for the initial and boundary conditions of the meteorological variables. Chemistry initial and boundary conditions were provided in 3 hour increments at a horizontal resolution of about 40 km x 40 km with 60 vertical levels from the surface up to 60 km by the European Centre for Medium-Range Weather Forecasts (ECMWF) operational model.

The physics, chemistry and emission options used in this study, as well as their corresponding references, are listed in Table 1. The most significant ones for this application are: the Rapid Radiative Transfer Model for General Circulation Model applications (RRTMG) scheme for longwave and shortwave radiation (Iacono et al., 2008); the Revised Mesoscale Model version 5 Monin–Obukhov scheme for surface layer (Jiménez et al., 2012); the Unified Noah land-surface model for land surface (Tewari et al., 2004); land use provided by the Moderate-resolution Imaging Spectroradiometer (MODIS) with spatial resolution and 20 different classes; the Yonsei University scheme for the boundary layer (Hong et al., 2006); the Morrison



2-moment scheme for microphysics (Morrison et al., 2009) and the Grell-Freitas ensemble convective scheme (Grell et al.,
130 2014).

We simulated atmospheric chemistry using the Regional Atmospheric Chemistry Model (RACM) coupled with the Modal
Aerosol Dynamics model for Europe/Volatility Basis Set (MADE/VBS) aerosol scheme, which treats the organic gas/particle
partitioning within a spectrum of volatilities (Ahmadov et al., 2012). The RACM includes 21 stable inorganic species (4
being intermediates), 32 stable organic species (4 of which are primarily of biogenic origin). In addition, RACM includes
135 237 chemical reactions (23 of which are photolysis). MADE/VBS has an advanced SOA module based on VBS approach
to simulate concentrations of the main organic and inorganic gas/particle partitions within a spectrum of volatilities using
saturation vapor concentrations as surrogates for volatility. It also includes less complex aqueous reactions (sulfate - SO_4 and
nitrate - NO_3 wet deposition) following CMAQ methodology (Sarwar et al., 2011). MADE/VBS has a four-bin VBS with
the SOA precursor yields based on previous smog chamber studies under both high- and low- NO_x conditions (Murphy and
140 Pandis, 2009; Ahmadov et al., 2012). Yields are for four volatility bins with saturation concentrations of 1, 10, 100, and 1000
 $\mu\text{g m}^{-3}$, and represent aerosol modes – Aitken ($< 0.1 \mu\text{m}$), accumulation ($0.1\text{--}1 \mu\text{m}$) and coarse ($> 1 \mu\text{m}$).

We used the approach by Fast et al. (2006), according to Mie theory (Mie, 1908), in order to account for aerosol radiative
properties such as absorption and scattering coefficients, SSA and g_{aer} . These properties are then transferred to the RRTMG
shortwave radiation scheme in order to calculate the corresponding radiative forcing. In addition, the feedback effects of clouds
145 on aerosol size and composition via aqueous-phase chemistry (Sarwar et al., 2011) as well as wet scavenging processes (Easter
et al., 2004) are considered.

Simulations were conducted in order to analyze how Manaus emissions affect SOA production and aerosol optical proper-
ties over the Amazon. We considered two scenarios: (i) Manaus on, which represents anthropogenic emissions and background
emissions from initial and boundary conditions; (ii) Manaus off, which represents a background scenario, dominated by bio-
150 genic emissions, with anthropogenic contribution coming from the boundary conditions.

2.2.1 Anthropogenic Emissions

Anthropogenic emissions were calculated using the Rafee et al. (2017) inventory, which considers emissions of all classes of
mobile (light-duty, heavy-duty vehicles and motorcycles) and stationary (thermal power plants (TPPs) and Refineries) sources.
Both components were calculated according to emission factors estimates based on experiments conducted inside road traffic
155 tunnels in São Paulo (Martins et al., 2006; Sánchez-Ccoyllo et al., 2009; Brito et al., 2013), providing the only vehicle emission
factor measurements available in Brazil. Fine particle matter emission fractionation into size and chemical classes were based
on studies developed for São Paulo (Ynoue and Andrade, 2004; Miranda and Andrade, 2005; Albuquerque et al., 2012).

2.2.2 Biogenic Emissions

Biogenic emissions were calculated online using the Model of Emissions of Gases and Aerosols from Nature (MEGAN)
160 version 2 (Guenther et al., 2006). Based on driving variables such as ambient temperature, solar radiation, leaf area index, and



Table 1. WRF-Chem simulations configuration used in this study

Simulation time: 2014-3-8 00 UTC to 2014-3-15 00 UTC	
Attributes	Model configurations
Grid resolution	dx = dy = 3 km
nx, ny, nz	200 x 150 x 51
Time step	10 s
Vertical resolution	51 layers from surface to 100 hPa (~16 km)
Physical options	
Radiation	Long/shortwave RRTMG scheme (Iacono et al., 2008)
Land surface	Unified Noah land-surface model (Tewari et al., 2004)
Surface layer	Revised Mesoscale Model version 5 Monin–Obukhov scheme (Jiménez et al., 2012)
Boundary layer	Yonsei University scheme (Hong et al., 2006)
Cloud microphysics	Morrison 2-moment (Morrison et al., 2009)
Cumulus clouds	Grell–Freitas ensemble scheme (Grell et al., 2014)
Chemical options	
Gas-phase chemistry	Updated RACM version with chemical reactions for sesquiterpenes (Papiez et al., 2009)
Aerosol module	MADE/VBS (Ahmadov et al., 2012)
Aerosol activation	Abdul-Razzak and Ghan scheme (Abdul-Razzak and Ghan, 2000)
Photolysis	TUV (Madronich, 1987)
Meteorological IC and BC	National Center for Environmental Prediction Final Analysis (NCEP-FNL)
Chemical IC and BC	European Centre for Medium-Range Weather Forecasts (ECMWF)
Emissions sources	
Biogenic	Model of Emissions of Gases and Aerosols from Nature (Guenther et al., 2006)
Anthropogenic	Emission inventory developed by Rafee et al. (2017)

plant functional types, this model estimates the net terrestrial biosphere emission rates for different trace gases and aerosols with a global coverage of $\approx 1 \text{ km}^2$ spatial resolution.

2.3 Observed Data

We used in situ real-time measurement at several GoAmazon2014/5 surface sites (see Fig. 1b). The particle scattering coefficient (σ_s) was measured using a 3-wavelength Nephelometer (450, 550 and 700nm; TSI 3563 Integrating Nephelometer). Particle absorption coefficient (σ_a) was measured at the T3 site with a 7-wavelength Magee AE31 Aethalometer that operates at $\lambda = 370, 430, 470, 520, 565, 700$ and 880 nm and was subjected to the correction scheme outlined by Rizzo et al. (2011). The observed (σ_a) values have been interpolated to the nephelometer's wavelengths to allow a proper comparison and calculation of the intensive parameters, such as SSA. The BC mass concentration at the T3 site was estimated using AE31 measurements of



170 the absorption coefficient at 880 nm and a mass absorption cross section (MAC) section of $7.77 \text{ m}^2 \text{ g}^{-1}$ (Drinovec et al., 2015).
At ATTO, the BC concentration was measured using a Thermo Environment MAAP 5012 (Thermo) using a σ_a at 637nm and
a MAC of $6.6 \text{ m}^2 \text{ g}^{-1}$, the absorption data was corrected according to Müller et al. (2011). Organic and inorganic submicron
aerosol mass loadings were measured with a Time of Flight Aerosol Mass Spectrometer (ToF-AMS) (de Sá et al., 2018). Mix-
ing ratios of ozone (O_3) and CO were obtained with a 49i O_3 Analyzer (Thermo Environment) and a $\text{N}_2\text{O}/\text{CO}$ Analyzer (Los
175 Gatos Research - LGR). Meteorological observations was measured by a Vaisala WXT520. Observed data was averaged at
1-hour intervals for comparison it with the WRF. Standard temperature and pressure (STP) corrections were also applied to all
measurements. We also used aircraft measurements of σ_a from the DoE Gulfstream 1 (G-1), as part of the GoAmazon2014/5
experiment (Shilling et al., 2018; Martin et al., 2016), measured using a 3-wavelength (461, 522 and 648nm) Particle/Soot
Absorption Photometer (PSAP) from Radiance Research.

180 2.3.1 GoAmazon2014/5 Experiment

The Observations and Modeling of the Green Ocean Amazon experiment GoAmazon2014/5 was designed to understand how
aerosol and cloud life cycles are influenced by the pollutant outflow from Manaus into the tropical rain forest (Martin et al.,
2016). The experiment used a set of detailed aerosol, trace gas and cloud measurements at six different sites (see Fig. 1b) in
order to better understand the atmospheric processes caused by the interaction between urban pollution emissions with volatile
185 organic compounds (VOCs) emitted from the forest, and the environmental impacts on the natural microphysical properties of
clouds and aerosols, such as optical properties and particle size distributions (Gu et al., 2017; Fraund et al., 2017).

3 Results and Discussion

3.1 Meteorological Analysis

To study the impact that Manaus pollution plume has on SOA production aerosol optical properties in the area downwind
190 of Manaus, meteorological conditions, especially temperature, humidity and PBL height, must be properly characterized and
represented in the WRF-Chem model. Comparisons at the T3 site between observed and simulated hourly variations of accu-
mulated total precipitation, 2 m temperature, 2 m relative humidity, 10 m wind speed, and PBL height (SI Figs. S1 and S2)
show that the model performs well in terms of diurnal representation and trends. Simulated temperature and humidity tend to
be underestimated (mean bias (MB) = -0.5 and -1.6, respectively), with a short delay between peak observed (11:00 LT) and
195 simulated (15:00 LT) values. The simulation has difficulties in obtaining the observed maximum temperature (see SI Fig. S1a).
According to statistical indices (SI Table 1), the correlation coefficient (r) and Root Mean Square Error (RMSE) show consis-
tent results for relative humidity ($r = 0.7$ and $\text{RMSE} = 1.8$), temperature ($r = 0.8$ and $\text{RMSE} = 0.4$) and wind speed ($r = 0.7$ and
 $\text{RMSE} = 0.2$). The relative humidity profile agrees well with ground base measurements, but the simulated values exhibit the
diurnal minimum with a 3 hour delay. Individual calculations of performance statistics are presented in Supplementary Table
200 S1.



The Central Amazon region has unique topographic characteristics including the Amazon, Negro and Solimões rivers (Marinho et al., 2020), resulting in meteorological systems such as local circulations and the so called *friagem* events, which occur when a frontal system reaches the Central Amazon basin (Marengo et al., 1997; Lu et al., 2005), that have important influences on the local and mesoscale circulations (dos Santos et al., 2014; Pereira Oliveira and Fitzjarrald, 1993; Silva Dias et al., 2004).
205 That may affect the wind direction and air subsidence patterns. Figure S3 in the SI compares the simulated vertical wind component during night time at the T3 site. In the early morning hours (05 - 11 LT), downdraft movement is not sufficient at the T3 site to inhibit pollutant dispersion. However, during the night time (20 - 22 LT), the simulation captured an organic aerosol concentration peak (see Fig. 5a) consistent with the presence of downdraft movement and a temperature inversion at low levels (see SI Fig. S4) observed at the T3 site.

210 3.1.1 Background Conditions

Generally, global and regional models contain uncertainties associated with the wet/dry deposition scheme (Wang et al., 2015). For example, the BC residence time in the atmosphere is typically larger in global models than in the real atmosphere. During the wet season, the T0a site is upwind of Manaus and so has low anthropogenic influence. However, the T0a site receives sporadic air masses loaded with marine aerosol transported from the Atlantic Ocean, and dust outflows from the Sahara desert,
215 in general together with smoke from fires in West Africa (Ben-Ami et al., 2010; Andreae et al., 2012, 2015; Rizzolo et al., 2017; Pöhlker et al., 2018). Those air masses transported from Africa during the wet season occur when the ITCZ is shifted to the south of the central Amazonian Basin, allowing air masses from the Northern Hemisphere to reach the central portion of the Basin.

Looking at Figure 2, it is possible to observe that on March 2014 10th and 11th, BC (both simulated and observed) were
220 above expected levels ($0.1 \mu\text{gm}^{-3}$), consistent with coherent BC long range transport from west Africa (Moran-Zuloaga et al., 2018). During the 10th and the 11th, the simulation also follows the BC variability shown in the observed data. The simulation appears to do a reasonable job of representing the BC transport from West Africa. Figure 2 shows that the global model BC concentrations are also representative of the hours with the largest values during the 10th and 11th.

March 13th shows good agreement between simulated and observed data at T3. We can assess the simulations ability to
225 represent Amazonian background conditions comparing observed and simulated data from the region with very little anthropogenic influence during the wet season, as is the case for the T0a site. Given that, the simulation calculates background BC and O₃ with RMSE and MB consistent with observations, it is possible to determine the aerosol enrichment at the T3 site due to the Manaus plume. The background BC in the Amazon near the T0a site is representative of almost pristine continental regions. The average observed BC values are influenced by biogenic aerosol absorption, the global BC background as well
230 as by BC that is long range transported from Saharan dust and African biomass burning. The BC transported from Africa is episodic, depending on the ITCZ positioning, as well as the air mass trajectories from Africa to the Central Amazon. As we have several years of BC background measurements at the ATTO tower, it is possible to separate African episodic events from the rather constant regional BC concentrations that are relevant to compare with the modeled values under no anthropogenic influences (Artaxo et al., 2020).

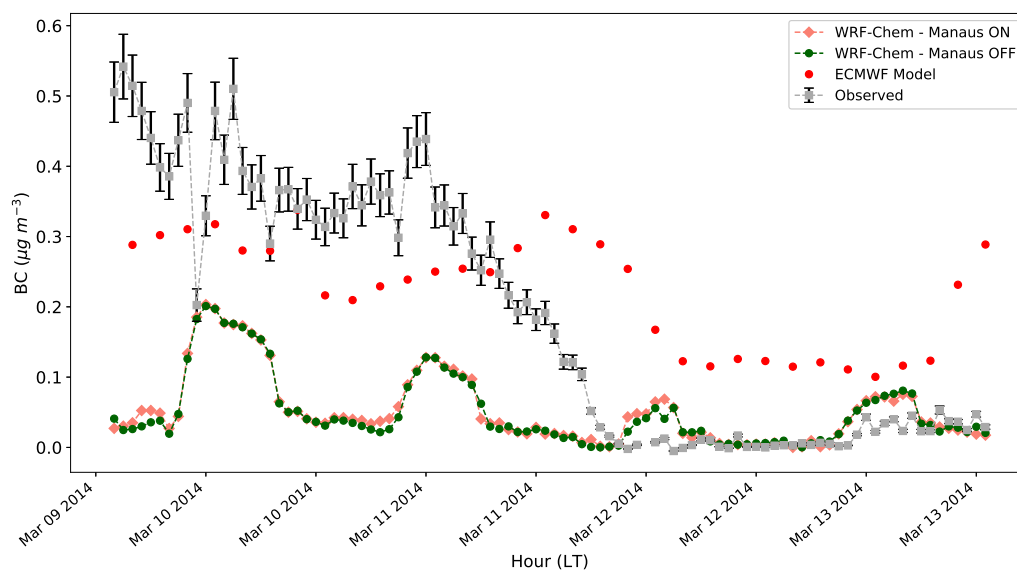


Figure 2. Observed and simulated surface BC concentration from March 10 to March 13, 2014 at the T0a site. Standard deviation bars are shown for each set of measurements. Events due to long range transport of Saharan dust and biomass burning emissions from West Africa are visible on the 10th and 11th (Moran-Zuloaga et al., 2018). The Manaus OFF (green) and Manaus ON (orange) simulations show BC concentrations simulated at a height of ca. 8 m above the surface. During BC transport event days, we can see that the simulation had the largest peaks, trying to represent the black carbon transport coming from west Africa. The global model contribution (red dots) also represents BC transport event days, showing the largest values during days 10th and 11th.

235 3.2 Chemical Analyses

To better understand the impact of the Manaus urban plume on SOA formation and mixing ratios at the T3 site during March 13, 2014 we must be able to separate time periods representing clean and polluted episodes, and compare observed and simulated values. Previous studies have developed methods to separate these episodes in the Amazon region (Palm et al., 2017; de Sá et al., 2018; Cirino et al., 2018).

240 In our analysis, with observed data from the GoAmazon2014/5 experiment (T3 site), adjusted cluster centroids were used to analyze clean and polluted conditions, during two months in the wet season (February and March 2014). We define three different clusters (i) low pollution (Low Pol), (ii) middle pollution (Mid Pol) and (iii) high pollution (High Pol) (see Table 2). We chose three different clusters at the T3 site because the pollution conditions arriving are heterogeneous. Our cluster analysis (see Fig. 3) was made with a fuzzy c-means (FCM) clustering algorithm (Bezdek et al., 1984). On March 13, 2014,
245 our analysis shows a day with mostly polluted conditions (at 10-17 LT). Previous work (Palm et al., 2017; de Sá et al., 2018) reported the same polluted conditions during this day.

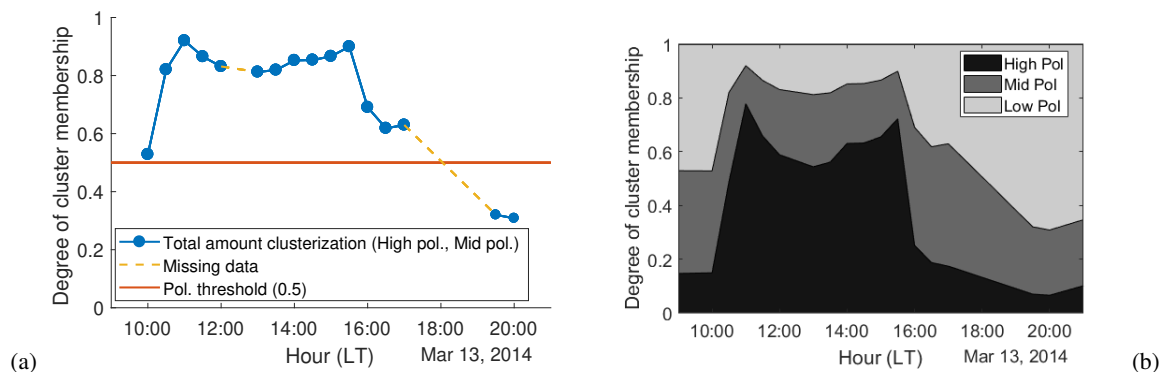


Figure 3. Results of FCM clusters analysis during March 13, 2014 from 10:00 to 20:00 LT. **(a)** Total clusterization considering polluted conditions with degree of cluster membership > 0.5 . **(b)** Degree of membership in each of the three clusters. The sum of degrees of membership across all clusters is unity. Background conditions are abbreviated as “Low Pol”, intermediate conditions as “Mid Pol” and polluted conditions are abbreviated as “High Pol”.

Table 2. Cluster centroids used to analyze clean and polluted conditions.

Cluster Centroids for March Day 13th						
Clusters	PM _{2.5} conc. num. (cm ⁻³)	CO (ppbv)	O ₃ (ppbv)	BC (ng/m ⁻³)	NO _y (ppbv)	SO ₄ (μg/m ⁻³)
Low Pol.	1304	117	11	43	0.71	0.16
Mid. Pol.	2566	123	15	99	1.39	0.29
High Pol.	5329	124	26	144	2.28	0.43

Because the concentration values of High Pol and Mid Pol, episodes are substantially larger than those at Low Pol we distinguish time periods representing clean episodes as Low Pol and polluted episodes as High Pol and Mid Pol. Quantitatively we separate clean from polluted episodes with the degree of cluster membership. When membership for Low Pol is > 0.5 , we consider this a clean episode. When the sum of Mid Pol and High Pol membership is > 0.5 we consider this a polluted episode. Initially, we attempted clustering with only two clusters (one for clean and one for polluted episodes), but were unable to separate polluted from background conditions. In this case the nominally background cluster had high black carbon (BC) and NO_y concentrations.

Given the abundance of BVOCs in the Amazon region (Alves et al., 2016; Yáñez-Serrano et al., 2020), we expect O₃ to be especially sensitive to changes in NO_x emission. This can be seen in Figure 4a; 4e, which shows high O₃ and low NO_x values downwind of Manaus. According to the WRF-Chem chemical mechanism, isoprene is rapidly oxidized by hydroxyl radicals (OH) to form peroxy radicals (HO₂) in a few hours (Ahmadov et al., 2012). The T1 site has a low isoprene concentration, since as the Manaus plume passes through forest regions with high isoprene production, the high plume NO_x concentration oxidizes the isoprene. This can be seen in Figure 4, where the Manaus plume consumes the isoprene around the T3 site, producing O₃



260 and HO₂. Because the enhancement of HO₂ radicals occurs downwind of Manaus (such as at the T3 site), the concentrations of NO_x are significantly lower (higher) than the values in Manaus (downwind in the forest), leading to a significant enhancement of O₃ (ca. 8 – 30 ppbv (Fig. 4a)). Because NO_x and isoprene emissions vary in different regions, our results suggest that NO_x in southeastern Manaus (Rafee et al., 2017) has important impacts on the O₃ concentration in the Manaus urban area. This is primarily due to the rapid reactions of radicals with NO_x, which deplete the radicals.

265 The O₃ values are highest during the day as VOC production peaks and solar radiation is available for the photo-chemical processes that produce O₃ (Graham et al., 2003a, b; Chen et al., 2015; Schultz et al., 2017). The O₃ enhancement 8 to 300 km downwind of Manaus suggests that the interaction between forest biogenic emissions and the pollution from Manaus could have an important impact on the chemical production of O₃ (Fig. 4a). The interaction between anthropogenic and biogenic trace gases has strong regional characteristics, such the ones found near Manaus. They also depend on the distributions of
270 BVOCs and anthropogenic NO_x. O₃ mixing ratios downwind of Manaus under the influence of anthropogenic pollution were also reported by Trebs et al. (2012) and were on average 31 ± 14 ppbv, with peak values of 60 ppbv at a distance of 19 km downwind of Manaus. Our simulations showed an O₃ average of 30 ± 11 ppbv at the T3 site (70 km downwind of Manaus) with high peak values of 148 ppbv in regions northwest of Manaus (Fig. 4a). Manaus pollution plume influence on O₃ production is clearly observed in the surrounding area, predominantly to the west and northwest of Manaus.

275 In regions downwind of Manaus, the simulations showed O₃ concentrations extending more than 300 km downwind. It is also interesting to note the lower O₃ values around T1, which are represented in both observed (ca. 8 ppbv on average) and simulated (ca. 12 ppbv on average) data (Fig. 4a). O₃ with ca. 8 ppbv on average is uncommonly low for a metropolis of nearly 1.8 million people. The agreement between observed and simulated O₃ values around T1 indicates that the chemistry there is being successfully reproduced by the simulation. Our explanation for this anomaly is that VOCs are abundant all around
280 Manaus (Kuhn et al., 2010; Alves et al., 2016) and HO_x and O₃ are low despite having high NO_x in a typically VOC limited regime. We hypothesize that in areas with very high NO_x emissions (averaging 129.02 ppbv), such as the power plant cluster surrounding T1 (Fig. 4e), radicals react quickly with NO_x (NO_x + OH → HNO₃). This depletes the O₃, creating radicals, causing a decrease in O₃ formation. Conversely, downwind of Manaus, the radicals last long enough to form O₃ and we observe an increase in O₃ formation, as well as an increase in HO₂ radicals (Fig. 4c).

285 Our results imply that the high NO_x conditions within Manaus affect the O₃ formation around Manaus, decreasing O₃ production within the city and providing a great enhancement downwind of Manaus (Fig. 4a). The wind direction is predominantly from the northeast, which allows the plume to be transported to the T2 and T3 sites and allowing the pollution plume to have a great impact on the surrounding areas (Martin et al., 2017). Interestingly, our results show that when O₃ concentrations change by a factor of between 2 and 4, oxidation and NO_x levels may be affected, and consequently, the rate and SOA production
290 efficiency may be impacted, by decreasing the reacted BVOCs and SOA formation downwind of Manaus.

According to Figure 5a, the simulated organic PM_{2.5} at the T3 site has one of the highest values during the first hours of March 13, 2014 (2 to 4, LT), with the largest contribution coming from primary anthropogenic organic aerosol (POA). We suggest that the large contributions of BC and CO emissions, coming from Manaus (Fig. S7 in the SI) together with a prevailing northeast wind direction, are the most plausible explanations why simulated total organics present high values

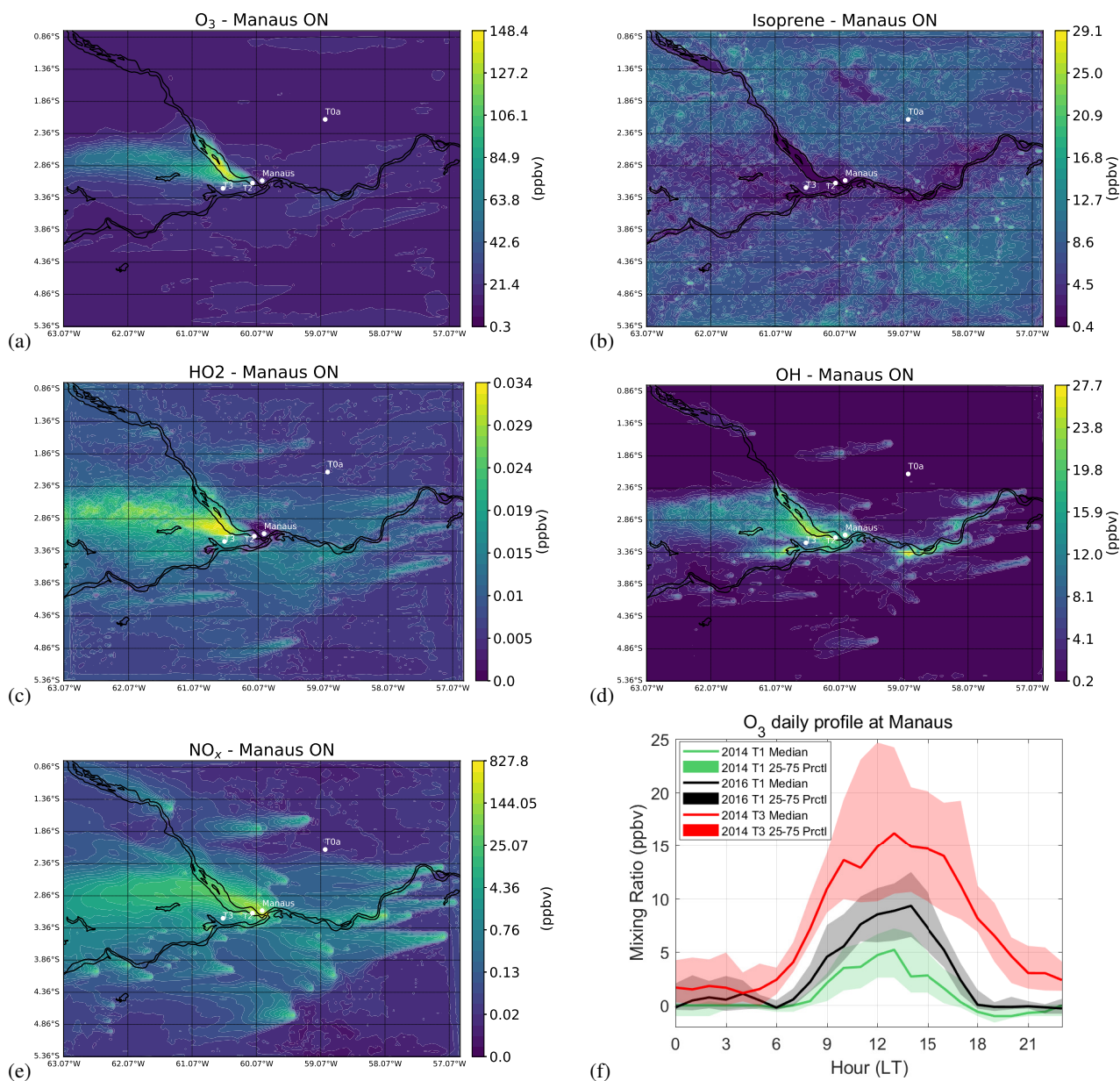


Figure 4. Temporal mean (06 to 15 LT March 13th) spatial distribution of simulated surface level concentrations of (a) O₃, (b) Isoprene, (c) HO₂, (d) OH, (e) NO_x and (f) daily median O₃ profile for the month of March (wet season) at T1 during 2014 (green line), 2016 (black line) and at the T3 site during 2014 (red line). The red, gray and green shaded areas show the 25th to 75th percentiles of the respective median line.

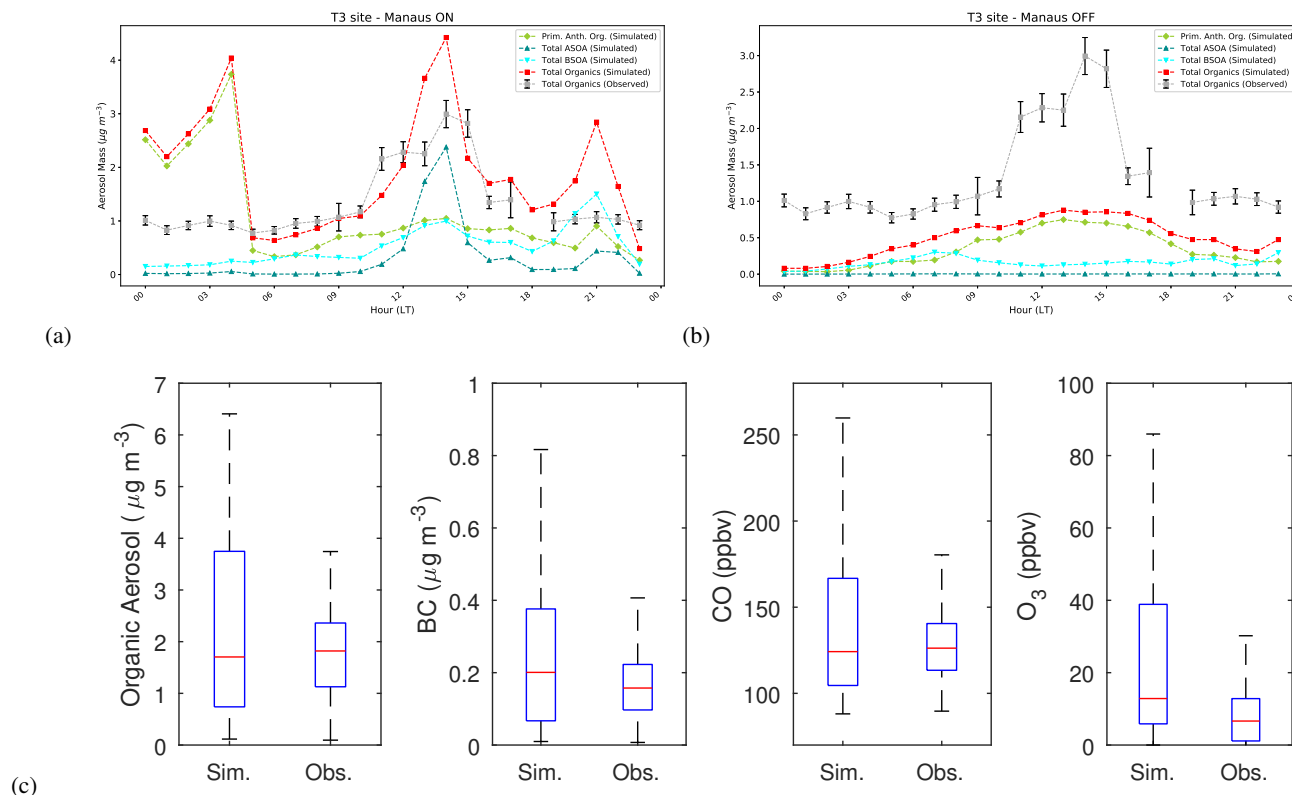


Figure 5. Times series and box plot comparison of measured and WRF-Chem-simulated surface level gases and aerosols at the T3 site. Contributions from simulated primary anthropogenic organic, BSOA and ASOA to total OA as simulated by WRF-Chem in the case (a) with and (b) without anthropogenic emissions on March 13, 2014 at the T3 site. (c) Comparison between observed and simulated surface level gases and aerosols. Box plot of simulated and observed organics, BC, CO and O₃ from March 9 to 13, 2014 at the T3 site. Median values are shown in red lines and the blue box indicates data between the 25th and 75th percentiles.

295 during the first hours of the day with an high POA peak during the first hours of March 13, 2014 (2 to 4, LT). The BC and CO contributions can end up reaching the T3 site, increasing the POA amount. In addition, the simulated BC concentration also showed simultaneously high values during the first hours of March 13, 2014 (2 to 4, LT) (Fig. S5 in the SI).

Between 10 and 16 LT there is an increase in the total organic aerosol concentration, which was successfully reproduced by our simulation. This evolution of the organic aerosol concentration was expected on that day due to the Manaus plume arriving at the T3 site (Shilling et al., 2018). This increase is mostly due to a sharp increase in anthropogenic SOA (ASOA) peaking at 15 LT, as well as the BSOA and POA at the same time. The highest value (4.4 $\mu\text{g m}^{-3}$) of simulated total organics occurred at 14 LT (Fig. 5a), and is comprised of mostly the SOA component, with increases in BSOA contributing 1.0 $\mu\text{g m}^{-3}$ (22.6%), ASOA 2.4 $\mu\text{g m}^{-3}$ (53.9%) and POA 1.04 $\mu\text{g m}^{-3}$ (23.5%). Conversely, when the simulation is run with anthropogenic emissions turned off, the total organic aerosol simulated at 14 LT is 0.9 $\mu\text{g m}^{-3}$, with BSOA contributing 0.14 $\mu\text{g m}^{-3}$ (16.3%), ASOA



305 $0.02 \mu\text{g m}^{-3}$ (2.3%) and POA $0.7 \mu\text{g m}^{-3}$ (81.4%). We attribute most of the difference in total organic aerosol between simulations with and without anthropogenic emissions to the ASOA amount, related the Manaus plume contributions. The same analysis, now considering the entire day of March 13th, shows a contribution coming mostly from POA of $26.4 \mu\text{g m}^{-3}$ (57.1%), BSOA $12.4 \mu\text{g m}^{-3}$ (26.8%) and ASOA $7.4 \mu\text{g m}^{-3}$ (16%). Considering the immensely complex mixture of organic aerosol particle and gas phase, VOCs and other species in continuous evolution in the atmosphere, and the large number of
310 chemical reactions with oxidant species such as OH (day-time) and NO_3 (nighttime) (Kuhn et al., 2010), we emphasize that there may be a relationship between BSOA and ASOA simulated peaks (see Fig. 5a) and the O_3 peak at 15 LT (Fig. S6 in the SI), since those chemical reactions are associated with the production of tropospheric O_3 and also oxygenated VOCs (Bela et al., 2016).

A third total organic aerosol simulated peak is observed between 20 and 21 LT (see Fig. 5a). The simulated peak may be
315 explained by the transport of air pollutants from the regions south of the T3 site (Fig. S8 in the SI). We propose two possible explanations for this phenomenon. Our first explanation involves the Negro River breeze effect. Since most thermal power plants and the Issac Sabbá refiner REMAN are located near the banks of the Negro and Solimões rivers (Rafee et al., 2017), the plume transport could be influenced by the river breeze circulation, which defines the trajectory of pollutants. It may be that, between 19 to 21 LT (Fig. S8 in the SI), the wind direction was affected by the Negro River breeze effect due the horizontal
320 thermal gradient caused by the different energy partitioning of the water and land surfaces. Consistent with dos Santos et al. (2014), the water surface temperature of the Negro River starts to increase in the afternoon (13 LT), affecting the vertical heat and mass transport. Our second explanation is that there is an air subsidence pattern at the T3 site between 19 and 22 LT (see SI Fig. S3). At 20 LT T3 site presents a saturation trend from 850 m to 900 m and also from 520 m to 600 m with temperature and dew-point temperature close to each other, creating a dry air region (see Fig. S4 in the SI), and consequently, air subsidence
325 (see Fig. S4b in the SI). This causes upward movement inhibition, which confines the atmospheric pollutants to low levels, impeding their spread.

An example of the differences between the measured and modeled concentration distributions is shown for organics, BC, CO and O_3 in Fig. 5c. Both simulated and observed BC show a median value of $0.2 \mu\text{g m}^{-3}$, demonstrating that our simulation represents BC well. The same behavior is shown for OA and CO with simulated and observed median values of $1.8 \mu\text{g m}^{-3}$ and
330 122 ppbv, respectively. However, the simulation presets a larger range of values compared with observations. The simulations present some high peaks not seen in the observed data, such as the ones in BC (see Fig. S5 in the SI) and OA, with a high contribution coming from POA emission factor (see Fig. 5a). Both have peaks in the early morning on March 13, 2014. In addition, the simulation shows a median O_3 value of ca. 12 ppbv (observed 7 ppbv). Conversely, looking at just 10 to 17 LT on March 2014, which represents an exemplary day with pollution contributions at the T3 site coming from Manaus (Shilling et al., 2018), both simulated and observed O_3 present high median values, 38 ppbv and 30 ppbv, respectively. This agreement of the observed and simulated median values during a day with polluted conditions, particularly noting the uncertainties in emissions (speciation, spatial and temporal distribution), measurements, boundary conditions, meteorological component and other input parameterization of the model are low on the 13th. Overall, the comparisons of the median measured and predicted

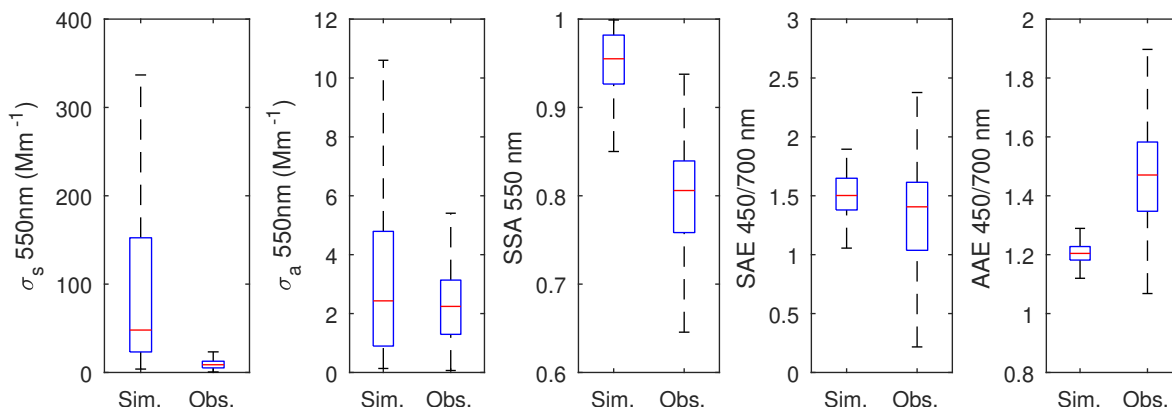


Figure 6. Comparisons between observed and simulated aerosol optical properties. Box plot of simulated and observed SSA, SAE, AAE, scattering and absorption coefficients from 9 to 13 March 2014 at the T3 site. Median values are shown in red lines and the blue box indicates data between the 25th and 75th percentiles.

chemical concentrations are satisfactory, with the best match obtained in OA (observed $1.8 \mu\text{g m}^{-3}$; simulated $1.7 \mu\text{g m}^{-3}$),
340 CO (observed 124 ppbv; simulated 126 ppbv) and BC (observed $0.201 \mu\text{g m}^{-3}$; simulated $0.203 \mu\text{g m}^{-3}$).

3.3 Variability of Amazonian Aerosol Optical Properties

Understanding how optical properties such as SSA and g_{aer} vary downwind of Manaus is key to understanding the impact of the pollution plume on radiative forcing, its contributions to the local radiative budget, its impacts on the hydrological cycle and unknown indirect consequences on photosynthesis rates. These effects suggest the possibility of investigating aerosol
345 direct radiative effects (DREs) by examining g_{aer} , which presents, in general, higher values associated with stronger forward scattering of radiation by atmospheric aerosols (Korras-Carraca et al., 2015).

Figure 6 shows that the simulation overestimates the observed scattering coefficient by a factor 6. The overestimate in the observed scattering coefficient is due the fact that our WRF-Chem simulations are producing more SO_4 than in the real atmosphere, with 30% of the observed PM1 attributed to SO_4 in the accumulation mode (Fig. S11 in the SI). Observed scattering
350 coefficient values are significantly lower than simulated likely due to decreases in the aerosol loading during the transect, modulated by the effects of dilution of gases and particles in the air. On the other hand, the median simulated absorption coefficient of 2.2 Mm^{-1} is in good agreement with the observed median value of 2.4 Mm^{-1} . We observe the simulated SSA being affected by the simulated scattering coefficient overestimation. Comparing simulated and observed SAE values, we again have good agreement between the simulation and observations, with the simulation representing the mean size of the aerosol population
355 70 km downwind of Manaus quite well. These results are important for the plume aging mechanism discussed in Section 3.4. Additionally, the observed AAE is considerably higher than in our simulation. This suggests that the brown carbon component,

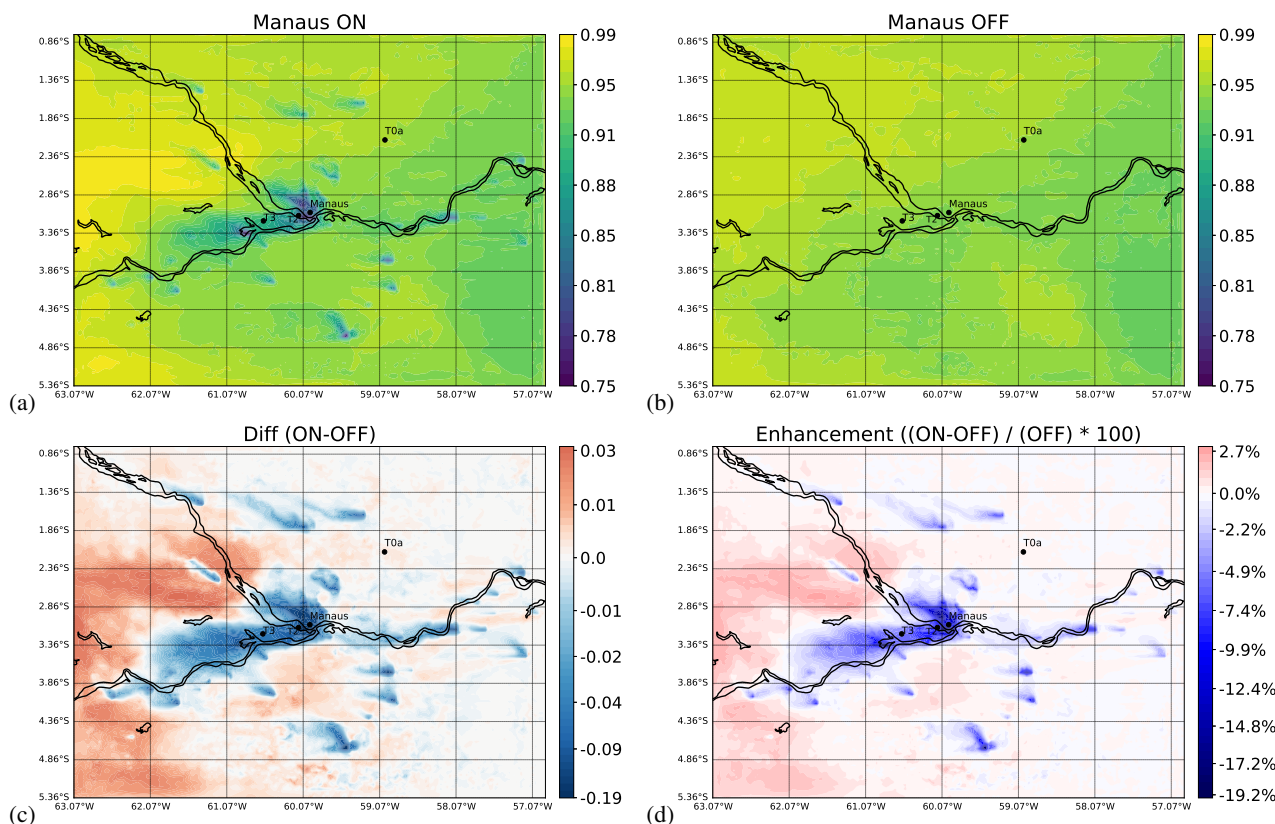


Figure 7. WRF-Chem simulated values of SSA in the presence or absence of Manaus emissions. (a) SSA when all emissions are ON. (b) SSA when just biogenic emissions are ON and anthropogenic emissions are OFF. (c) SSA difference between the two simulations with anthropogenic emissions turned ON and OFF i.e. (ON-OFF). (d) SSA enhancement (%) calculated from the two simulations with anthropogenic emissions turned ON/OFF i.e. $((ON-OFF)/OFF) \times 100$. WRF-Chem predictions are at ca. 8 m altitude, averaged over March 13, 2014 (00:00 – 23:00 LT.)

not accounted for our simulations, could have an critical effect on the AAE value, contributing to the lower median simulated AAE (1.2) compared with the median observed value (1.5).

3.3.1 Calculations and measurements of SSA

360 According to our simulation results, the Manaus plume interferes with the amount of radiation absorbed by the atmosphere, being responsible for an SSA reduction of approximately 10% at Manaus, 12% at the T2 site and 5.3% at the T3 site (see Fig. 7d). This indicates a large fraction of absorbing material present in the Manaus plume, potentially warming the local atmosphere. These regions are associated with thermal power plants (Medeiros et al., 2017), indicating that the vehicular emissions and stationary sources (refineries) are dominated by small absorbing particles like BC, while biogenic particles are mostly found in the coarse mode and efficiently scatter radiation due to their organic carbon-dominated composition.

365

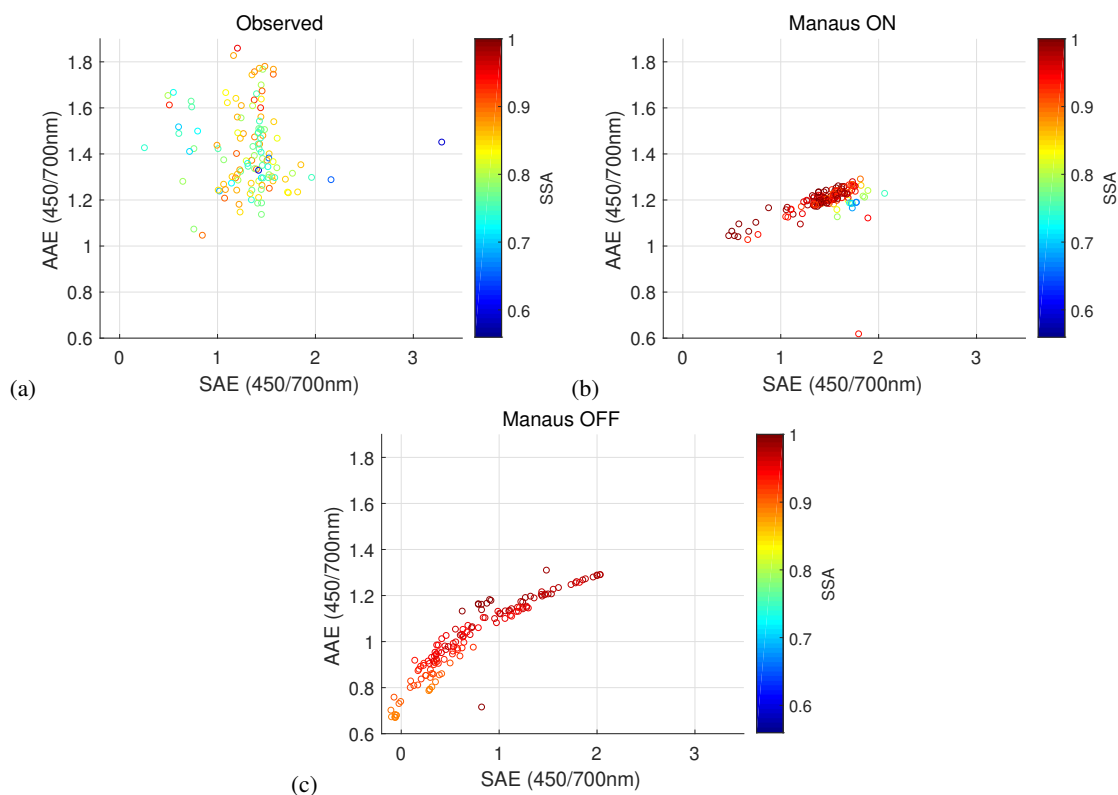


Figure 8. AAEs at the wavelength pair 470 nm and 660 nm as a function of the corresponding SAEs at the wavelength pair 470 nm and 660 nm), color-coded using the related SSA at the wavelength pair 470 nm and 660 nm). 1 h averaged instantaneous observed data values (a) from simultaneous nephelometer and aethalometer measurements from 9 to 14 March 2014. (b) 1 h averaged simulated values when all emissions are on. (c) 1 h average simulated values when just biogenic emissions are on and anthropogenic emissions are off.

During simulations with the Manaus pollution plume component turned on, average SSA values vary between 0.75 and 0.90 in regions downwind of Manaus. This represents the contribution from the interaction of urban aerosols with biogenic components of the forest. Similar results were found by Cirino et al. (2018) at the T3 site (0.80) and Ramachandran and Rajesh (2007) in western India (0.88), He et al. in China (0.80), Backman et al. (2012) in São Paulo, Brazil (0.76). These SSA values are associated with the formation of SOA aerosols which scatter radiation efficiently (Fig. S10 in the SI). The decrease in the SSA is associated with a significant fraction of aerosol loading from small particles of anthropogenic origin, e.g., BC. The average simulated and observed SSA on 550 nm values during March 13, 2014 at the T3 site were 0.86 ± 0.09 and 0.78 ± 0.09 , respectively.

370



3.3.2 Calculations of AAE and SAE

375 Figure 8 shows the simulated and observed SAE and AAE distributions from 9 to 14 March 2014. The simulation with anthropogenic emissions is mostly characterized by $1.0 < \text{AAE} < 1.3$ and $1.0 < \text{SAE} < 2.0$, corresponding to a large OC particle contribution, including primary and secondary components (POC and SOC, respectively) (Cazorla et al., 2013). Additionally, the simulated SAE (Manaus on) when variability ranges between 1 to 1.8, indicates a contribution of fine and absorbing particles, which increases the SAE (see Fig. 8).

380 In general, these SAE and AAE values show that the values in simulation with anthropogenic emissions are, on average, associated with the fine fraction of $\text{PM}_{2.5}$ sampled particles. In contrast, some values are mostly associated with large-size $\text{PM}_{2.5}$ particles ($\text{SAE} < 1$), consistent with the Manaus plume not having a strong influence on the T3 site during those days. Conversely, the SAE with anthropogenic emissions (see Fig. 8b) shows a range between 0.5 and 2.1, values associated with the presence of fine aerosols originating from industrial activities in Manaus and the thermal power plants (TTPs) located in
385 the surrounding area. The simulation with the Manaus plume turned off (see Fig. 8c) shows a coarse mode predominance, with SAE values varying mainly between 0.0 and 1.5. Thus, we can assume those values have a large OC contribution because of the predominance of aerosol coming from coarse mode biogenic sources.

The observed AAE values in the simulation without anthropogenic emissions express a large variability (1.1 to 1.8) compared with the ones from simulation with anthropogenic emissions (1 to 1.3). This behavior is assumed being caused by the lack of
390 a brown carbon component in the aerosol population in our simulation. When the anthropogenic emissions are off, the SAE variability is mostly related with the significant contribution from large aerosol, as already mentioned (Cazorla et al., 2013; Seinfeld and Pandis, 2016; Romano et al., 2019).

3.3.3 Asymmetry Parameter

G_{aer} is an important optical property in radiative transfer, climate and general circulation models (Korras-Carraca et al. (2015)).
395 The, g_{aer} describes the angular distribution of scattered radiation and determines whether the particles scatter radiation preferentially forwards or backwards (Boucher (2015)).

Figure 9 (a) shows low 600nm g_{aer} values (0.64) that could be associated with industrial activities such as TTPs as well as biomass burning in nearby areas. A region of special interest is between Manaus and T3, since it hosts a large variety of mixing interactions between anthropogenic, biogenic and dust aerosols (e.g., Artaxo et al., 2002; Saturno et al., 2018; Martin et al.,
400 2016; Rizzo et al., 2013). In this region it can be seen that g_{aer} decreases by 8% compared when there is no anthropogenic emissions (see Fig. 9d). This is associated with the presence of fine anthropogenic aerosols transported from adjacent urban and industrial areas in the northwest, especially from central Manaus (Medeiros et al., 2017; Rafee et al., 2017; Shrivastava et al., 2019). Those smaller g_{aer} values are seen in places where a significant fraction of the aerosol loading comes from small size particles of anthropogenic origin, with the smallest values appearing over the regions containing industrial activities.
405 Previous studies (Cirino et al., 2018) have shown a period in the late afternoon around T3 in which particles with the smallest geometric diameter (ca. 50 nm) were observed, and the same period coincides with smaller g_{aer} found in simulations for the

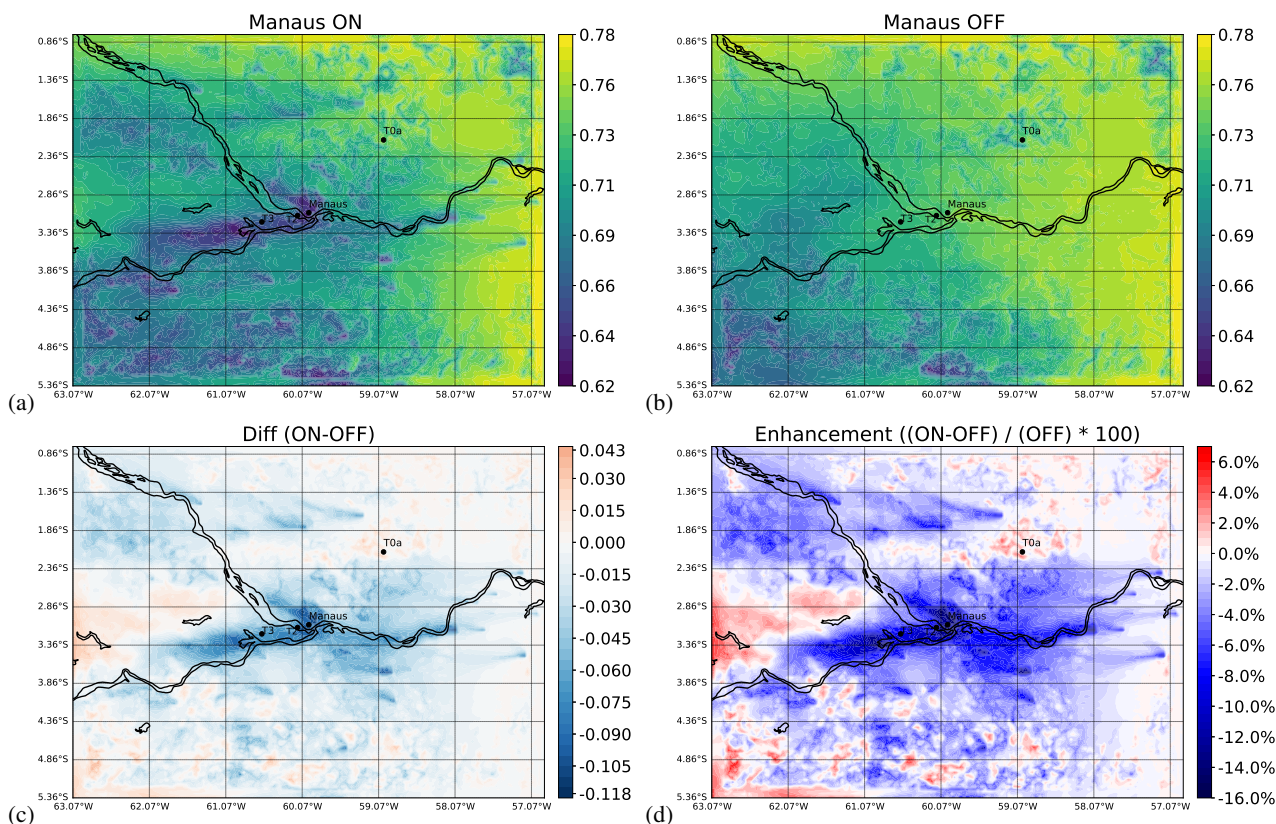


Figure 9. WRF-Chem simulated values of 600nm g_{aer} in the presence or absence of Manaus emissions. (a) g_{aer} when all emissions are on. (b) g_{aer} when just biogenic emissions are on and anthropogenic emissions are off. (c) g_{aer} difference between the two simulations with anthropogenic emissions turned on and off i.e. (ON-OFF). (d) g_{aer} (%) enhancement calculated from the two simulations when anthropogenic emissions turned on and off i.e. $((ON-OFF)/OFF) \times 100$. WRF-Chem predictions are at ca. 8 m altitude, averaged over March 13, 2014 (0 to 23 LT).

same station (see Fig. 9a). On the other hand, g_{aer} when anthropogenic emissions are off, g_{aer} has predominately large values varying between 0.75 and 0.76 at 300 nm, 0.73 and 0.75 at 400 nm, 0.71 and 0.74 at 600 nm and 0.63 and 0.71 at 1000 nm. These values indicate strong forward scattering of radiation by atmospheric aerosols and are related with the presence of coarse biogenic particles. According to the obtained results, anthropogenic emissions decrease g_{aer} values by between 2% and 16%, especially in regions with large mobile and stationary anthropogenic activities. Those smaller values can induce modifications of the DREs.

3.3.4 Irradiance

In regions like the Amazon with sufficiently high levels of NO_x , and VOCs such as isoprene and monoterpene, an enhanced formation of near surface O_3 is expected. Solar radiation is another element that contributes to photochemical activity and,

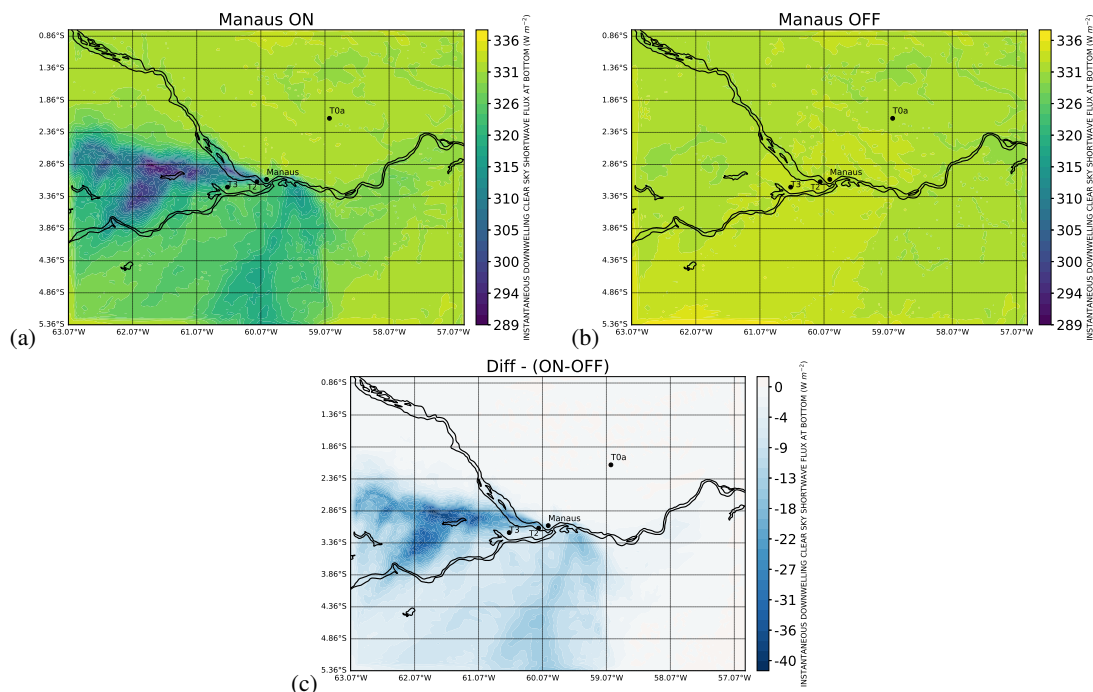


Figure 10. WRF-Chem simulated mean incoming solar radiation (instantaneous downwelling clear sky shortwave flux at bottom: SWDNBC) in $W m^{-2}$ in the presence and absence of Manaus emissions. (a) SWDNBC when all emissions are on. (b) SWDNBC when biogenic emissions are on and anthropogenic emissions are off. (c) SWDNBC difference between the simulations with and without anthropogenic emissions, i.e. ON-OFF.

consequently, the formation of O_3 . According to Figure 10c, it is possible to notice that even in regions presenting average decreased surface downward shortwave flux values of ca. $20 W m^{-2}$ due to the presence of anthropogenic emissions near T2 and T3, not enough to reduce the enhanced formation of near surface O_3 (see Fig. 4a), which more than compensates for the effect of the comparatively reduced solar radiation there. The lower solar radiation over the west side of Manaus seen in simulations with anthropogenic emissions (see Fig. 10a) is accompanied by a general increase in mean O_3 values (see Fig. 4a). Studies of regional direct and indirect aerosol effects are important and still challenging due to their complexity making an accurate determination of the direct and indirect effects difficult (Forkel et al., 2012; Wang et al., 2015; Zhang et al., 2010).

In our simulations, we considered both direct and indirect aerosol effects during the wet season in the Amazon region. Incoming shortwave radiation at the surface is predicted to drop by up to ca. $-40 W m^{-2}$ due the direct aerosol effect. In regions within and up to ca. 100 km south-west of Manaus, Figure 10c shows an aerosol cooling effect with maximum SWDNBC values ca. $-40 W m^{-2}$. The same behavior can also be seen in the region north-west of the T3 site. The aerosol cooling effect is mostly related with SOA production caused by the interaction between VOCs and NO_x . When the Manaus plume reaches regions downwind of the city, as seen on March 13, 2014, with few clouds, low precipitation and biomass burning, the plume has a cooling effect on the region as the plume evolves. The SWDNBC (clear sky) variable was used in this study to investigate the



430 aerosol radiative effect on the surface due limitations for simulate the cloud coverage on Amazonian region. Also, the results
founded in this paper have to be investigated deeply in order to better understand the effects on the diffuse and direct radiation.

3.4 Aging Plume Impact on the Optical Properties

In this section, we examine how aging of the Manaus plume may affect its optical properties. SSA initially has low values of
ca. 0.91, then increases after plume age 1 (7 LT). Some processes which affect SSA values as the plume ages are dilution, BC
435 deposition, SOA formation and the lensing effect (Holanda et al., 2020; Shrivastava et al., 2019; Cirino et al., 2018). The SSA
values in the plume continue to increase during the plume aging process, consistent with SOA (ASOA + BSOA) production in
the aging plume (see Fig. 11d). Our simulations show that, on March 13, 2014, the increase of SSA as the plume ages is mostly
related to a combination of an increase in SOA formation and BC dilution. Figure 11f shows that BC and CO diluted in similar
proportions, suggesting that, at this time scale, dilution is more important than deposition. When the plume is 3 hours old, total
440 organics reach ca. $11 \mu\text{g m}^{-3}$ and at that time the plume is north of the T3 site (see Fig. S12d in the SI). Similar results were
found by de Sá et al. (2018) at the T3 site.

During plume aging, a decrease of anthropogenic primary organic aerosol and a increase in SOA was observed, similar to
results reported by Shilling et al. (2018). The biggest contribution to total SOA during the plume aging comes from anthro-
pogenic emissions, ca. 70% of the total SOA. SOA production increases rapidly and saturates at plume age 4, indicating that
445 it is a challenge to represent these processes in tropical regions with global models, especially without correct treatments of
sub-grid effects, such as the production of SOA. The simulated plume used in the tracking analysis traveled 160 km from
Manaus (Fig. S13 in the SI). The distance between T1 and T3 is around 70 km, so when the plume reaches that distance from
Manaus, it is ca. 3 hours old.

Figure 11b shows instantaneous downwelling clear sky shortwave flux at bottom with the Manaus plume turned on and off.
450 After 3 hours of plume aging, incoming solar radiation is reduced by ca. -15 W m^{-2} and is further reduced by about -30 W m^{-2}
after the plume is 7 hours old. This reduction by 3% of solar flux and the resulting increase in diffuse radiation results in a
significant increase in net primary productivity (Cirino et al., 2014; Rap et al., 2015). As the plume ages and dilutes, its impact
on the solar radiation remains constant. Between hours 7 and 9, although the plume's attenuation of incoming solar radiation
decreases in absolute terms, from ca. -32 W m^{-2} to -27 W m^{-2} , as a percentage, the plume's attenuation remains constant at
455 ca. 3%.

BC simulations at an altitude of ca. 500 m above the ground were evaluated using aircraft measurements from the Manaus
plume on March 13, 2014. For the most part, our simulation shows good agreement with the G1 measurements (SI Fig. S16,
in the SI), particularly for background conditions. The offset in the third and fourth peaks is due to differences between the
meteorological conditions of the simulation and reality. Similar offsets between simulations and observations were found by
460 Shrivastava et al. (2019).

As the plume ages SAE, begins to increase at 8 LT (after 2 hours of plume aging) and remains constant with values of ca.
1.17 until 13 LT (after 7 hours of plume aging). During this period, AAE is mostly close to 1, which can be explained by
increased concentrations of fine ($\text{SOA} > 15 \mu\text{g m}^{-3}$) and absorbing ($\text{BC} > 0.4 \mu\text{g m}^{-3}$) particles near Manaus. Similar results

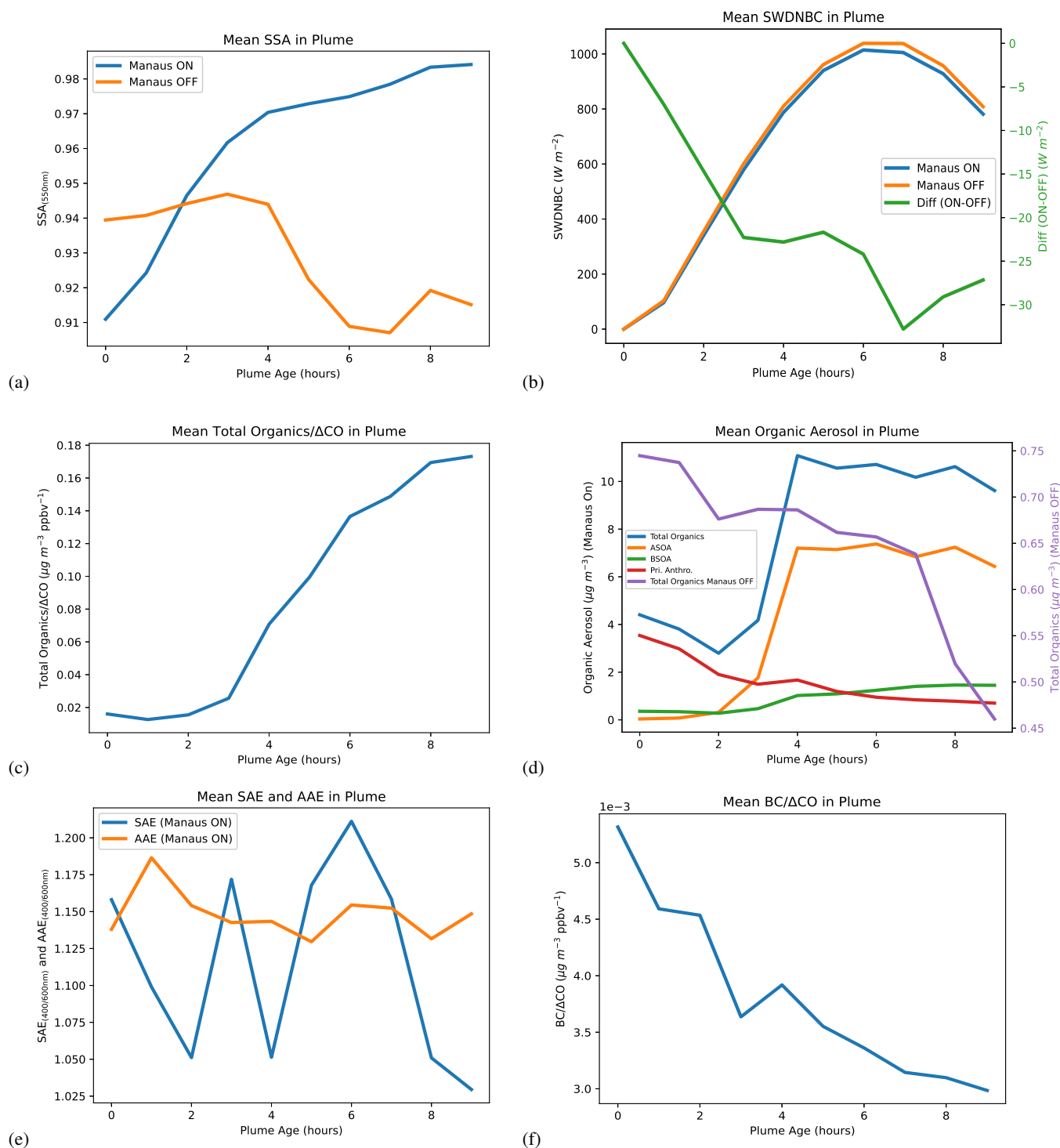


Figure 11. Simulated plume 100-500 m starting at Manaus 6 to 15 LT on March 13, 2014 in order to calculate the mean (a) SSA at 550nm, (b) Instantaneous downwelling clear sky shortwave flux at bottom ($W m^{-2}$), (c) Total organics ($\mu g m^{-3}$) normalized by ΔCO , (d) Organic aerosol ($\mu g m^{-3}$), (e) SAE and AAE and (f) BC ($\mu g m^{-3}$) normalized by ΔCO . The plume age represents the time the plume tracking started.



were found by Romano et al. (2019) in southeastern Italy from December 22, 2015 to March 30, 2016, with $1 < \text{AAE} < 1.5$
465 and $\text{SAE} > 1$ using the classification defined by Cappa et al. (2016).

4 Summary and conclusions

Numerical simulations with the WRF-Chem model were performed in order to investigate the impact of the Manaus plume on aerosol optical properties downwind of Manaus and how the plume aging process can affect those optical properties. We use the simulations to investigate the impact of anthropogenic emissions on SOA formation over the Amazon region during the wet
470 season and the effect of anthropogenic NO_x on O_3 production from O_3 precursors emitted by the forest. Aerosol characteristics have many impacts that could influence ecosystems on a regional scale. We selected March 13th, 2014 as a "golden day" (Shilling et al., 2018), to analyze the Manaus plume's influence at the T3 site and regions further downwind. During this day, the transport event brought elevated gas and aerosol concentrations from Manaus, associated with favorable meteorological conditions. According to our results, downwind of Manaus at the T3 site, the total organic aerosol mass increased by ca. 75%
475 ($0.5 - 2.0 \mu\text{g m}^{-3}$) when anthropogenic emissions were turned on. This increase in organic aerosol mass suggests the Manaus plume is primarily responsible for the changes in the physical and chemical aerosol population characteristics in those regions.

From model experiments, we conclude that the influence of the Manaus plume can reach areas up to 300 km downwind of Manaus, and provide a quantitative assessment of the effects urban pollution could cause to Amazonian forests surrounding urban centers. Overall, our simulations indicate that the aerosol impact of the Manaus plume increases irradiance values by
480 20% near the T3 site. We also separated the contributions of the different aerosol chemical components that contribute to our estimate of the total aerosol mass concentration and their impact on optical properties. Especially striking is the impact on O_3 formation. Due to the high NO_x concentrations present in Manaus, the simulations showed that increased O_3 production mostly occurs in the regions to the south-west of Manaus, where an atmosphere conducive to O_3 enhancement can be found.

According to our results, the lowest g_{aer} values were generally found in regions with a significant fraction of the aerosol load
485 coming from small size particles of anthropogenic origin, e.g., from TPPs and refineries in the Manaus region. Conversely, the largest g_{aer} values were observed over regions with aerosol dominated by large particles of biogenic origin (T0a site). Further investigations are necessary to determine if different sulfate amounts from anthropogenic emissions may change the strong direct effect for high aerosol particle concentrations. More ground-based aerosol and trace gas observations over the western Amazon region could help to evaluate the magnitude of the aerosol effect in this area.

This study contributes to the investigation of the optical properties of $\text{PM}_{2.5}$ over the Amazon region during the wet season. To assess the impact of Manaus emissions on SOA production, and consequently, on aerosol optical properties, WRF-Chem model runs were conducted with and without anthropogenic emissions. Assuming only biogenic emissions with boundary conditions from the global model, OA production decreased by 75% at the T3 site. This study also shows that on March 13, 2014, the aerosol aging process caused a gradual increase in SSA. Additionally, due to the deposition process, significantly
495 decreasing concentrations of BC are found during plume evolution. This process, combined with SOA formation, contributes to the increase in SSA as the plume ages. The results of this study demonstrate that uncertainties in coating processes of organic



aerosols involving BC particles also warrant additional study to better account for a possible decrease in SSA during the plume aging process. The results here also demonstrate that in order to precisely calculate the radiative forcing impact, it is important to take into account all SOA formation mechanisms, including VOC oxidation, especially for tropical forest regions like the Amazon. One action that may improve SOA model accuracy is to update some of the MEGAN model inputs when new data such as emission factors and vegetation coverage data becomes available. In addition, there are very few long term aircraft based ASOA and BSOA observations data and more observations could help validate the models and improve their accuracy.

Data availability. The GoAmazon2014/5 experiment data are available from the ARM website: <https://www.arm.gov/research/campaigns/amf2014goamazon> and from the Laboratory of Atmospheric Physics - LFA website: http://lfa.if.usp.br/ftp/public/LFA_Processed_Data/. The simulations and analysis code generated for this study are available upon request from JPN.

Author contributions. JPN, MMB and PA conceptualized and defined the methodology. JPN carried out the formal analysis and investigation of the model results with support from BM, MMB, ALB, HG, LVR, SC, HJB, MAF, MT, SAM and PA. ALVV, SAAR, HG and MMB supported the design and running of simulations. GGC, PA, LVR, MLB, BM and RAFS collected and curated the experimental data. JPN wrote the original draft and all authors discussed the results and commented on the paper.

Competing interests. The authors declare that they have no conflict of interest.

Acknowledgements. We acknowledge support from the Central Office of the Large-Scale Biosphere Atmosphere Experiment in Amazonia (LBA), coordinated by the National Institute of Amazonian Research (INPA) and the Amazonas State University (UEA), Amazonas, Brazil. JPN thanks the Brazilian Federal Agency for Support and Evaluation of Graduate Education (CAPES) for a graduate fellowship, linked to the doctoral program in Climate and Environment (CLIAMB) and for supporting 7 months of a visiting graduate student program at the NOAA Earth System Research Laboratory. JPN also thanks the Institute of Physics of the University of São Paulo (IFUSP) for student mobility and logistical support, and CIRES and NOAA ESRL for financial and logistical support. We thank Michael Trainer for providing support and knowledge during the research. We thank Manish Shrivastava for providing WRF-Chem simulation output for comparison with this work. We thank Steven Jefferts, Stefania Romisch and Samuel Brewer for facilitating communication between members of this collaboration. We are grateful to Bruno Takeshi, Luiz Cândido, Renata Teixeira and Delano Campos for instrument operation and data analysis. Finally, we thank Richard Tisinai for IT support. MAF acknowledges a scholarship from CNPq, Project 169842/2017-7, for supporting his PhD studies at the IFUSP, São Paulo, Brazil, and CAPES, Project 88887.368025/2019-00, for supporting 6 months of a visiting graduate student program at the Max Planck Institute for Chemistry, Mainz, Germany. BM acknowledges a scholarship from CNPq, Project 133393/2019-4, for supporting his Masters studies at the IFUSP, São Paulo, Brazil. HG acknowledges funding from CAPES through grant 1757/2017. PA acknowledges funding from FAPESP through grant 2017/17047-0.



525 *Financial support.* JPN has been supported by the Brazilian Federal Agency for Support and Evaluation of Graduate Education (CAPES) - Project Code 88882.444345/2018-01 and 88881.190103/2018-01.



References

- Abdul-Razzak, H. and Ghan, S. J.: A parameterization of aerosol activation: 2. multiple aerosol types, *J. Geophys. Res.*, 105, 6837–6844, <https://doi.org/10.1029/1999JD901161>, 2000.
- 530 Ahmadov, R., McKeen, S., Robinson, A., Bahreini, R., Middlebrook, A., De Gouw, J., Meagher, J., Hsie, E.-Y., Edgerton, Shaw, S., and Trainer, M.: A volatility basis set model for summertime secondary organic aerosols over the eastern United States in 2006, *J. Geophys. Res.*, 117, D06301, <https://doi.org/10.1029/2011JD016831>, 2012.
- Albuquerque, T. T. A., Andrade, M. F., and Ynoue, R. Y.: Characterization of atmospheric aerosols in the city of São Paulo, Brazil: comparisons between polluted and unpolluted periods, *Environ. Monit. Assess.*, 184(2), 969–984, 2012.
- 535 Alves, E. G., Jardine, K., Tota, J., Jardine, A., Yáñez-Serrano, A. M., Karl, T., Tavares, J., Nelson, B., Gu, D., Stavrou, T., Martin, S., Artaxo, P., Manzi, A., and Guenther, A.: Seasonality of isoprenoid emissions from a primary rainforest in central Amazonia, *Atmos. Chem. Phys.*, 16, 3903–3925, <https://doi.org/10.5194/acp-16-3903-2016>, 2016.
- Andreae, M., Artaxo, P., Beck, V., Bela, M., Freitas, S., Gerbig, C., Longo, K., Munger, J., Wiedemann, K., and Wofsy, S.: Carbon monoxide and related trace gases and aerosols over the Amazon Basin during the wet and dry seasons, *Atmos. Chem. Phys.*, 12, 6041–6065, <https://doi.org/10.5194/acp-12-6041-2012>, 2012.
- 540 Andreae, M. O., Acevedo, O. C., Araújo, A., Artaxo, P., Barbosa, C. G. G., Barbosa, H. M., Joel, B., Carbone, S., Chi, X., Cintra, B. B. L., da Silva, N. F., Dias, N. L., Dias-Júnior, C. Q., Ditas, F., Ditz, R., Godoi, A. F. L., Godoi, R. H. M., Heimann, M., Hoffmann, T., Kesselmeier, J., Koenemann, T., Krüger, M. L., Lavric, J. V., Manzi, A. O., Lopes, A. P., Martins, D. L., Mikhailov, E. F., Moran-Zuloaga, D., Nelson, B. W., Nölscher, A. C., Santos Nogueira, D., Piedade, M. T. F., Pöhlker, C., Pöschl, U., Quesada, C. A., Rizzo, L. V., Ro, C.-U., Ruckteschler, N., Sá, L. D. A., de Oliveira Sá, M., Sales, C. B., dos Santos, R. M. N., Saturno, J., Schöngart, J., Sörgel, M., de Souza, C. M., de Souza, R. A. F., Su, H., Targhetta, N., Tóta, J., Trebs, I., Trumbore, S., van Eijck, A., Walter, D., Wang, Z., Weber, B., Williams, J., Winderlich, J., Wittmann, F., Wolff, S., and Yáñez-Serrano, A. M.: The Amazon Tall Tower Observatory (ATTO): overview of pilot measurements on ecosystem ecology, meteorology, trace gases, and aerosols, *Atmos. Chem. Phys.*, 15, 10723–10776, <https://doi.org/10.5194/acp-15-10723-2015>, 2015.
- 550 Artaxo, P., Maenhaut, W., Storms, H., and Van Grieken, R.: Aerosol characteristics and sources for the Amazon Basin during the wet season, *J. Geophys. Res.-Atmos.*, 95(D10), 16971–16985, <https://doi.org/10.1029/JD095iD10p16971>, 1990.
- Artaxo, P., Yamasoe, M., Martins, J., Kocinas, S., Car-Vallo, S., and Maenhaut, W.: Case study of atmospheric measurements in Brazil : aerosol emissions from Amazon Basin fires, in: *Environmental Sciences Research Report*, edited by Crutzen, P. J. and Goldammer, J., vol. 13, pp. 139–158, Wiley, 1993.
- 555 Artaxo, P., Gerab, F., Yamasoe, M. A., and Martins, J. V.: Fine mode aerosol composition at three long-term atmospheric monitoring sites in the Amazon Basin, *J. Geophys. Res.-Atmos.*, 99, 22857–22868, <https://doi.org/10.1029/94JD01023>, 1994.
- Artaxo, P., Martins, J. V., Yamasoe, M. A., Procópio, A. S., Pauliquevis, T. M., Andreae, M. O., Guyon, P., Gatti, L. V., and Leal, A. M. C.: Physical and chemical properties of aerosols in the wet and dry seasons in Rondônia, Amazonia, *J. Geophys. Res.*, 107, 8081, <https://doi.org/10.1029/2001JD000666>, 2002.
- 560 Artaxo, P., Rizzo, L. V., Brito, J. F., Barbosa, H. M., Arana, A., Sena, E. T., Cirino, G. G., Bastos, W., Martin, S. T., and Andreae, M. O.: Atmospheric aerosols in Amazonia and land use change: from natural biogenic to biomass burning conditions, *Faraday discussions*, 165, 203–235, <https://doi.org/10.1039/C3FD00052D>, 2013.



- Artaxo, P., Hansson, H.-C., Andreae, M. O., Bäck, J., Alves, E. G., Barbosa, H. M. J., Bender, F., Bourtsoukidis, E., Carbone, S., Chi, J., Decesari, S., Després, V. R., Ditas, F., Ezhova, E., Fuzzi, S., Hasselquist, N. J., Heintzenberg, J., Holanda, B. A., Guenther, A., Hakola, H., Heikkinen, L., Kerminen, V.-M., Kontkanen, J., Krejci, R., Kulmala, M., Lavric, J., de Leeuw, G., Lehtipalo, K., Machado, L. A. T., McFiggans, G., Franco, M. A. M., Mohr, C., Morgan, W., Nilsson, M. B., Peichl, M., Petäjä, T., Praß, M., Pöhlker, C., Pöhlker, M. L., Pöschl, U., Randow, C. V., Riipinen, I., Rinne, J., Rizzo, L. V., Rosenfeld, D., Dias, M. A. F. S., Sogacheva, L., Stier, P., Swietlicki, E., Sörgel, M., Tunved, P., Virkkula, A., Wang, J., Weber, B., Yáñez-Serrano, A. M., Zieger, P., Mikhailov, E., Smith, J., and Kesselmeier, J.: Tropical and Boreal Forest – Atmosphere Interactions: A Review, *Tellus B: Chemical and Physical Meteorology*, 2020.
- 565 Backman, J., Rizzo, L. V., Hakala, J., Nieminen, T., Manninen, H. E., Morais, F., Aalto, P. P., Siivola, E., Carbone, S., Hillamo, R., Artaxo, P., Virkkula, A., Petäjä, T., and Kulmala, M.: On the diurnal cycle of urban aerosols, black carbon and the occurrence of new particle formation events in springtime São Paulo, Brazil, *Atmos. Chem. Phys.*, 12, 11 733–11 751, <https://doi.org/10.5194/acp-12-11733-2012>, 2012.
- Bela, M. M., Barth, M. C., Toon, O. B., Fried, A., Homeyer, C. R., Morrison, H., Cummings, K. A., Li, Y., Pickering, K. E., Allen, D. J., Yang, Q., Wennberg, P. O., Crounse, J. D., St. Clair, J. M., Teng, A. P., O’Sullivan, D., Huey, L. G., Chen, D., Liu, X., Blake, D. R., Blake, N. J., Apel, E. C., Hornbrook, R. S., Flocke, F., Campos, T., and Diskin, G.: Wet scavenging of soluble gases in DC3 deep convective storms using WRF-Chem simulations and aircraft observations, *J. Geophys. Res.-Atmos.*, 121, 4233–4257, <https://doi.org/10.1002/2015JD024623>, 2016.
- 575 Ben-Ami, Y., Koren, I., Rudich, Y., Artaxo, P., Martin, S., and Andreae, M.: Transport of Saharan dust from the Bodele Depression to the Amazon Basin: a case study, *Atmos. Chem. Phys. Discuss*, 10, 4345, <https://doi.org/10.5194/acp-10-7533-2010>, 2010.
- Bezdek, J. C., Ehrlich, R., and Full, W.: FCM: The fuzzy c-means clustering algorithm, *Computers & Geosciences*, 10, 191–203, [https://doi.org/10.1016/0098-3004\(84\)90020-7](https://doi.org/10.1016/0098-3004(84)90020-7), 1984.
- Boucher, O.: *Atmospheric Aerosols: Properties and Climate Impacts*, Springer Netherlands, <https://doi.org/10.1007/978-94-017-9649-1>, 2015.
- 585 Brito, J., Rizzo, L. V., Herckes, P., Vasconcellos, P., Caumo, S. E. S., Fornaro, A., Ynoue, R. Y., Artaxo, P., and Andrade, M. F.: Physical–chemical characterisation of the particulate matter inside two road tunnels in the São Paulo Metropolitan Area, *Atmos. Chem. Phys.*, 13, 12 199–12 213, <https://doi.org/10.5194/acp-13-12199-2013>, 2013.
- Brito, J., Rizzo, L., Morgan, W., Coe, H., Johnson, B., Haywood, J., Longo, K., Freitas, S., Andreae, M., and Artaxo, P.: Ground-based aerosol characterization during the South American Biomass Burning Analysis (SAMBBA) field experiment, *Atmos. Chem. Phys.*, 14, 12 069–12 083, <https://doi.org/10.5194/acp-14-12069-2014>, 2014.
- 590 Cappa, C. D., Kolesar, K. R., Zhang, X., Atkinson, D. B., Pekour, M. S., Zaveri, R. A., Zelenyuk, A., and Zhang, Q.: Understanding the optical properties of ambient sub-and supermicron particulate matter: results from the CARES 2010 field study in northern California, *Atmos. Chem. Phys.*, 16, 6511–6535, <https://doi.org/10.5194/acp-16-6511-2016>, 2016, 2016.
- Cazorla, A., Bahadur, R., Suski, K., Cahill, J. F., Chand, D., Schmid, B., Ramanathan, V., and Prather, K.: Relating aerosol absorption due to soot, organic carbon, and dust to emission sources determined from in-situ chemical measurements., *Atmos. Chem. Phys.*, 13, <https://doi.org/10.5194/acpd-13-3451-2013>, 2013.
- Chen, Q., Farmer, D., Rizzo, L. V., Pauliquevis, T., Kuwata, M., Karl, T. G., Guenther, A., Allan, J. D., Coe, H., Andreae, M. O., Pöschl, U., Jimenez, J. L., Artaxo, P., and Martin, S. T.: Submicron particle mass concentrations and sources in the Amazonian wet season (AMAZE-08), *Atmos. Chem. Phys.*, 15, 3687–3701, <https://doi.org/10.5194/acp-15-3687-2015>, 2015.



- 600 Cirino, G., Brito, J., Barbosa, H. M. J., Rizzo, L. V., Tunved, P., de Sá, S. S., Jimenez, J. L., Palm, B. B., Carbone, S., Lavric, J., Souza, R. A. F., Wolff, S., Walter, D., Tota, J., Oliveira, M. B. L., Martin, S. T., and Artaxo, P.: Observations of Manaus urban plume evolution and interaction with biogenic emissions in GoAmazon 2014/5, *Atmos. Environ.*, 191, 513–524, <https://doi.org/10.1016/j.atmosenv.2018.08.031>, 2018.
- Cirino, G. G., Souza, R. A. F., Adams, D. K., and Artaxo, P.: The effect of atmospheric aerosol particles and clouds on net ecosystem
605 exchange in the Amazon, *Atmos. Chem. Phys.*, 14, 6523–6543, <https://doi.org/10.5194/acp-14-6523-2014>, 2014.
- Cosgrove, B. A., Lohmann, D., Kenneth, M. E., Houser, P. R., Wood, E. F., Schaake, J. C., Robock, A., Marshall, C., Sheffield, J., Duan, Q., Lifeng, L., Higgins, W. R., Pinker, R. T., Tarpley, D. J., and J., M.: Real-time and retrospective forcing in the North American Land Data Assimilation System (NLDAS) project, *J. Geophys. Res.-Atmos.*, 108, <https://doi.org/10.1029/2002JD003118>, 2003.
- de Sá, S. S., Palm, B. B., Campuzano-Jost, P., Day, D. A., Hu, W., Isaacman-VanWertz, G., Yee, L. D., Brito, J., Carbone, S., Ribeiro,
610 I. O., Cirino, G. G., Liu, Y. J., Thalman, R., Sedlacek, A., Funk, A., Schumacher, C., Shilling, J. E., Schneider, J., Artaxo, P., Goldstein, A. H., Souza, R. A. F., Wang, J., McKinney, K. A., Barbosa, H., Alexander, M. L., Jimenez, J. L., and Martin, S. T.: Urban influence on the concentration and composition of submicron particulate matter in central Amazonia, *Atmos. Chem. Phys.*, 18, 12 185–12 206, <https://doi.org/10.5194/acp-18-12185-2018>, 2018.
- de Sá, S. S., Rizzo, L. V., Palm, B. B., Campuzano-Jost, P., Day, D. A., Yee, L. D., Wernis, R., Isaacman-VanWertz, G., Brito, J., Carbone,
615 S., Liu, Y. J., Sedlacek, A., Springston, S., Goldstein, A. H., Barbosa, H. M. J., Alexander, M. L., Artaxo, P., Jimenez, J. L., and Martin, S. T.: Contributions of biomass-burning, urban, and biogenic emissions to the concentrations and light-absorbing properties of particulate matter in central Amazonia during the dry season, *Atmos. Chem. Phys.*, 19, 7973–8001, <https://doi.org/10.5194/acp-19-7973-2019>, 2019.
- dos Santos, M. J., Silva Dias, M. A. F., and Freitas, E. D.: Influence of local circulations on wind, moisture, and precipitation close to Manaus City, Amazon Region, Brazil, *J. Geophys. Res.-Atmos.*, 119, 13 233–13 249, <https://doi.org/10.1002/2014JD021969>, 2014.
- 620 Draxler, R. R.: Demonstration of a global modeling methodology to determine the relative importance of local and long-distance sources, *Atmos. Environ.*, 41, 776–789, <https://doi.org/10.1016/j.atmosenv.2006.08.052>, 2007.
- Drinovec, L., Močnik, G., Zotter, P., Prévôt, A. S. H., Ruckstuhl, C., Coz, E., Rupakheti, M., Sciare, J., Müller, T., Wiedensohler, A., and Hansen, A. D. A.: The "dual-spot" Aethalometer: an improved measurement of aerosol black carbon with real-time loading compensation, *Atmos. Meas. Tech.*, 8, 1965–1979, <https://doi.org/10.5194/amt-8-1965-2015>, 2015.
- 625 Dubovik, O. and King, M. D.: A flexible inversion algorithm for retrieval of aerosol optical properties from Sun and sky radiance measurements, *J. Geophys. Res.-Atmos.*, 105, 20 673–20 696, 2000.
- Easter, R. C., Ghan, S. J., Zhang, Y., Saylor, R. D., Chapman, E. G., Laulainen, N. S., Abdul-Razzak, H., Leung, L. R., Bian, X., and Zaveri, R. A.: MIRAGE: Model description and evaluation of aerosols and trace gases, *J. Geophys. Res.-Atmos.*, 109, <https://doi.org/10.1029/2004JD004571>, 2004.
- 630 Fast, J. D., Gustafson, W. I., Easter, R. C., Zaveri, R. A., Barnard, J. C., Chapman, E. G., Grell, G. A., and Peckham, S. E.: Evolution of ozone, particulates, and aerosol direct radiative forcing in the vicinity of Houston using a fully coupled meteorology-chemistry-aerosol model, *J. Geophys. Res.-Atmos.*, 111, D21305, <https://doi.org/10.1029/2005JD006721>, 2006.
- Fisch, G., Marengo, J. A., and Nobre, C. A.: Uma revisão geral sobre o clima da Amazônia, *Acta amazônica*, 28, 101–101, 1998.
- Forkel, R., Werhahn, J., Hansen, A. B., McKeen, S., Peckham, S., Grell, G., and Suppan, P.: Effect of aerosol-radiation feedback on regional
635 air quality—A case study with WRF/Chem, *Atmos. Environ.*, 53, 202–211, <https://doi.org/10.1016/j.atmosenv.2011.10.009>, 2012.



- Fraund, M., Pham, D. Q., Bonanno, D., Harder, T., Wang, B., Brito, J., de Sá, S. S., Carbone, S., China, S., Artaxo, P., Martin, S., Pöhlker, C., Andreae, M., Laskin, A., Gilles, M., and Moffet, R.: Elemental mixing state of aerosol particles collected in Central Amazonia during GoAmazon2014/15, *Atmosphere*, 8, 173, <https://doi.org/10.3390/atmos8090173>, 2017.
- 640 Graham, B., Guyon, P., Maenhaut, W., Taylor, P. E., Ebert, M., Matthias-Maser, S., Mayol-Bracero, O. L., Godoi, R. H. M., Artaxo, P., Meixner, F. X., Lima Moura, M. A., Eça D'Almeida Rocha, C. H., Van Grieken, R., Glovsky, M. M., Flagan, R. C., and Andreae, M. O.: Composition and diurnal variability of the natural Amazonian aerosol, *J. Geophys. Res.-Atmos.*, 108 (D24), 4765, <https://doi.org/10.1029/2003JD004049>, 2003a.
- Graham, B., Guyon, P., Taylor, P. E., Artaxo, P., Maenhaut, W., Glovsky, M. M., Flagan, R. C., and Andreae, M. O.: Organic compounds present in the natural Amazonian aerosol: Characterization by gas chromatography–mass spectrometry, *J. Geophys. Res.-Atmos.*, 108 (D24), 4766, <https://doi.org/10.1029/2003JD003990>, 2003b.
- 645 Grell, G. A., Peckham, S. E., Schmitz, R., McKeen, S., Frost, G., Skamarock, W. C., and Eder, B.: Fully coupled “online” chemistry within the WRF model, *Atmos. Environ.*, 39, 6957–6975, <https://doi.org/10.1016/j.atmosenv.2005.04.027>, <http://dx.doi.org/10.1016/j.atmosenv.2005.04.027>, 2005.
- Grell, G. A., Freitas, S. R., et al.: A scale and aerosol aware stochastic convective parameterization for weather and air quality modeling, *Atmos. Chem. Phys.*, 14, 5233–5250, <https://doi.org/10.5194/acp-14-5233-2014>, 2014.
- 650 Gu, D., Guenther, A. B., Shilling, J. E., Yu, H., Huang, M., Zhao, C., Yang, Q., Martin, S. T., Artaxo, P., Kim, S., Seco, R., Stavrou, T., Longo, K. M., Tóta, J., de Souza, R. A. F., Vega, O., Liu, Y., Shrivastava, M., Alves, E. G., Santos, F. C., Leng, G., and Hu, Z.: Airborne observations reveal elevational gradient in tropical forest isoprene emissions, *Nature communications*, 8, 1–7, <https://doi.org/10.1038/ncomms15541>, 2017.
- 655 Guenther, A., Karl, T., Harley, P., Wiedinmyer, C., Palmer, P., and Geron, C.: Estimates of global terrestrial isoprene emissions using MEGAN (Model of Emissions of Gases and Aerosols from Nature), *Atmos. Chem. Phys.*, 6, 3181–3210, <https://doi.org/10.5194/acp-6-3181-2006>, 2006.
- Haywood, J. and Boucher, O.: Estimates of the direct and indirect radiative forcing due to tropospheric aerosols: A review, *Rev. Geophys.*, 38 (4), 513–543, <https://doi.org/10.1029/1999RG000078>, 2000.
- 660 He, X., Li, C. C., Lau, A. K. H., Deng, Z. Z., Mao, J. T., Wang, M. H., and Liu, X. Y.: An intensive study of aerosol optical properties in Beijing urban area., *Atmos. Chem. Phys.*, 9, 8903–8915.
- Holanda, B. A., Pöhlker, M. L., Saturno, J., Sörgel, M., Ditas, J., Ditas, F., Wang, Q., Donth, T., Artaxo, P., Barbosa, H. M. J., Borrmann, S., Braga, R., Brito, J., Cheng, Y., Dollner, M., Kaiser, J. W., Klimach, T., Knote, C., Krüger, O. O., Fütterer, D., Lavrič, V. J., Ma, N., Machado, L. A. T., Ming, J., Morais, F. G., Paulsen, H., D., S., Schlager, H., Schneider, J., Su, H., Weinzierl, B., Walser, A., Wendisch, 665 M., Ziereis, H., Zöger, M., Pöschl, U., Andreae, M. O., and Pöhlker, C.: Influx of African biomass burning aerosol during the Amazonian dry season through layered transatlantic transport of black carbon-rich smoke, *Atmos. Chem. Phys.*, 20, 4757–4785, 2020.
- Hong, S.-Y., Noh, Y., and Dudhia, J.: A new vertical diffusion package with an explicit treatment of entrainment processes, *Monthly weather review*, 134, 2318–2341, <https://doi.org/10.1175/MWR3199.1>, 2006.
- Iacono, M. J., Delamere, J. S., Mlawer, E. J., Shephard, M. W., Clough, S. A., and Collins, W. D.: Radiative forcing by 670 long-lived greenhouse gases: Calculations with the AER radiative transfer models, *J. Geophys. Res.-Atmos.*, 113, D13103, <https://doi.org/10.1029/2008JD009944>, 2008.
- Jiménez, P. A., Dudhia, J., González-Rouco, J. F., Navarro, J., Montávez, J. P., and García-Bustamante, E.: A revised scheme for the WRF surface layer formulation, *Mon. Weather Rev.*, 140, 898–918, <https://doi.org/10.1175/MWR-D-11-00056.1>, 2012.



- Korras-Carraca, M., Hatzianastassiou, N., Matsoukas, C., Gkikas, A., and Papadimas, C.: The regime of aerosol asymmetry parameter over Europe, the Mediterranean and the Middle East based on MODIS satellite data: evaluation against surface AERONET measurements, *Atmos. Chem. Phys.*, 15, 13 113, 2015.
- Kuhn, U., Ganzeveld, L., Thielmann, A., Dindorf, T., Schebeske, G., Welling, M., Sciare, J., Roberts, G., Meixner, F., Kesselmeier, J., et al.: Impact of Manaus City on the Amazon Green Ocean atmosphere: ozone production, precursor sensitivity and aerosol load, *Atmos. Chem. Phys.*, 10, 9251–9282, <https://doi.org/10.5194/acp-10-9251-2010>, 2010.
- 680 Lim, S., Lee, M., Kim, S.-W., Yoon, S.-C., Lee, G., and Lee, Y. J.: Absorption and scattering properties of organic carbon versus sulfate dominant aerosols at Gosan climate observatory in Northeast Asia., *Atmos. Chem. Phys.*, 14, <https://doi.org/10.5194/acp-14-7781-2014>, 2014.
- Lu, L., Denning, A. S., da Silva-Dias, M. A., da Silva-Dias, P., Longo, M., Freitas, S. R., and Saatchi, S.: Mesoscale circulations and atmospheric CO₂ variations in the Tapajós Region, Pará, Brazil, *J. Geophys. Res.-Atmos.*, 110, 1–17, <https://doi.org/10.1029/2004JD005757>, 2005.
- 685 Madronich, S.: Photodissociation in the atmosphere: 1. Actinic flux and the effects of ground reflections and clouds, *J. Geophys. Res.-Atmos.*, 92, 9740–9752, <https://doi.org/10.1029/JD092iD08p09740>, 1987.
- Marengo, J. A., Nobre, C. A., and Culf, A. D.: Climatic impacts of “friagens” in forested and deforested areas of the Amazon basin, *Journal of Applied Meteorology*, 36, 1553–1566, [https://doi.org/10.1175/1520-0450\(1997\)036<1553:CIOFIF>2.0.CO;2](https://doi.org/10.1175/1520-0450(1997)036<1553:CIOFIF>2.0.CO;2), 1997.
- 690 Marinho, R. R., Filizola Junior, N. P., and Cremon, É. H.: Analysis of Suspended Sediment in the Anavilhanas Archipelago, Rio Negro, Amazon Basin, *Water*, 12, 1073, <https://doi.org/10.3390/w12041073>, 2020.
- Martin, S., Artaxo, P., Machado, L., Manzi, A., Souza, R., Schumacher, C., Wang, J., Andreae, M., Barbosa, H., Fan, J., et al.: Introduction: observations and modeling of the Green Ocean Amazon (GoAmazon2014/5), *Atmos. Chem. Phys.*, 16, <https://doi.org/10.5194/acp-16-4785-2016>, 2016.
- 695 Martin, S. T., Andreae, M. O., Althausen, D., Artaxo, P., Baars, H., Borrmann, S. H., Chen, Q., Farmer, D. K., Guenther, A. B., Gunthe, S. S., et al.: An overview of the Amazonian aerosol characterization experiment 2008 (AMAZE-08), Volume 10, Número 23, Pags. 11415–11438, <https://doi.org/10.5194/acp-10-11415-2010>, 2010.
- Martin, S. T., Artaxo, P., Machado, L., Manzi, A. O., Souza, R., Schumacher, C., Wang, J., Biscaro, T., Brito, J., Calheiros, A., et al.: The Green Ocean Amazon experiment (GoAmazon2014/5) observes pollution affecting gases, aerosols, clouds, and rainfall over the rain forest, *Bulletin of the American Meteorological Society*, 98, 981–997, <https://doi.org/10.1175/BAMS-D-15-00221.1>, 2017.
- 700 Martins, L. D., Andrade, M. F., Freitas, E. D., Pretto, A., Gatti, L. V., Albuquerque, É. L., Tomaz, E., Guardani, M. L., Martins, M. H., and Junior, O. M.: Emission factors for gas-powered vehicles traveling through road tunnels in São Paulo, Brazil, *Environmental science & technology*, 40, 6722–6729, 2006.
- Medeiros, A. S., Calderaro, G., Guimarães, P. C., Magalhaes, M. R., Morais, M. V., Rafee, S. A., Ribeiro, I. O., Andreoli, R. V., Martins, J. A., Martins, L. D., et al.: Power plant fuel switching and air quality in a tropical, forested environment, *Atmos. Chem. Phys. (Online)*, 17, <https://doi.org/10.5194/acp-2016-1113>, 2017.
- Mie, G.: Beiträge zur Optik trüber Medien, speziell kolloidaler Metallösungen, *Annalen der physik*, 330, 377–445, 1908.
- Miranda, R. M. and Andrade, M. F.: Physicochemical characteristics of atmospheric aerosol during winter in the São Paulo Metropolitan area in Brazil, *Atmos. Environ.*, 39, 6188–6193, 2005.



- 710 Moran-Zuloaga, D., Ditas, F., Walter, D., Saturno, J., Brito, J., Carbone, S., Chi, X., de Angelis, I. H., Baars, H., Godoi, R. H., et al.: Long-term study on coarse mode aerosols in the Amazon rain forest with the frequent intrusion of Saharan dust plumes, *Atmos. Chem. Phys.*, 18, 10 055–10 088, 2018.
- Morrison, H., Thompson, G., and Tatarskii, V.: Impact of cloud microphysics on the development of trailing stratiform precipitation in a simulated squall line: Comparison of one- and two-moment schemes, *Monthly weather review*, 137, 991–1007, <https://doi.org/10.1175/2008MWR2556.1>, 2009.
- 715 Müller, T., Henzing, J., Leeuw, G. d., Wiedensohler, A., Alastuey, A., Angelov, H., Bizjak, M., Collaud Coen, M., Engström, J., Gruening, C., et al.: Characterization and intercomparison of aerosol absorption photometers: result of two intercomparison workshops, <https://doi.org/10.5194/amt-4-245-2011>, 2011.
- Murphy, B. N. and Pandis, S. N.: Simulating the formation of semivolatile primary and secondary organic aerosol in a regional chemical transport model, *Environmental science & technology*, 43, 4722–4728, <https://doi.org/10.1021/es803168a>, 2009.
- 720 Nobre, C. A., Obregón, G. O., J. A., Fu, R., and Poveda, G.: Characteristics of Amazonian climate: Main features, *Amazonia and Global Change*, edited by: Keller, M., Bustamante, M., Gash, J., Silva Dias, P., *Geophys. Mon. Ser.*, 186, 149–162, <https://doi.org/10.1029/2002JD002911>, 2009.
- Palacios, R. d. S., Romera, K. S., Curado, L. F., Banga, N. M., Rothmund, L. D., Sallo, F. d. S., Morais, D., Santos, A. C., Moraes, T. J., 725 Morais, F. G., et al.: Long term analysis of optical and radiative properties of aerosols in the Amazon Basin, *Aerosol and Air Quality Research*, <https://doi.org/10.4209/aaqr.2019.04.0189>, 2020.
- Palm, B. B., Day, D. A., Jimenez, J. L., et al.: CCN activity and organic hygroscopicity of aerosols downwind of an urban region in central Amazonia: seasonal and diel variations and impact of anthropogenic emissions, *Atmos. Chem. Phys.*, 17, <https://doi.org/10.5194/acp-17-11779-2017>, 2017.
- 730 Palm, B. B., de Sá, S. S., Day, D. A., Campuzano-Jost, P., Hu, W., Seco, R., Sjostedt, S. J., Park, J.-H., Guenther, A. B., Kim, S., et al.: Secondary organic aerosol formation from ambient air in an oxidation flow reactor in central Amazonia, *Atmos. Chem. Phys. Discussions* (Online), 18, <https://doi.org/10.5194/acp-18-467-2018>, 2018.
- Papież, M. R., Potosnak, M. J., Goliff, W. S., Guenther, A. B., Matsunaga, S. N., and Stockwell, W. R.: The impacts of reactive terpene emissions from plants on air quality in Las Vegas, Nevada, *Atmos. Environ.*, 43, 4109–4123, <https://doi.org/10.1016/j.atmosenv.2009.05.048>, 735 2009.
- Pereira Oliveira, A. and Fitzjarrald, D. R.: The Amazon river breeze and the local boundary layer: I. Observations, *Boundary-Layer Meteorology*, 63, 141–162, <https://doi.org/10.1007/BF00705380>, 1993.
- Pöhlker, C., Walter, D., Paulsen, H., Könemann, T., Rodriguez-Caballero, E., Moran-Zuloaga, D., Brito, J., Carbone, S., Degrendele, C., Després, V. R., Ditas, F., Holanda, B. A., Kaiser, J. W., Lammel, G., Lavrič, J. V., Ming, J., Pickersgill, D., Pöhlker, M. L., Saturno, J., 740 Sörgel, M., Wang, Q., Weber, B., Wolff, S., Artaxo, P., Pöschl, U., and Andreae, M. O.: Land cover and its transformation in the backward trajectory footprint region of the Amazon Tall Tower Observatory, *Atmos. Chem. Phys.*, 19, 8425–8470, <https://doi.org/10.5194/acp-19-8425-2019>, 2019.
- Pöhlker, M. L., Ditas, F., Saturno, J., Klimach, T., Hrabec de Angelis, I., Araùjo, A., Brito, J., Carbone, S., Cheng, Y., Chi, X., Ditz, R., Gunthe, S. S., Kandler, K., Kesselmeier, J., Könemann, T., Lavrič, J. V., Martin, S. T., Mikhailov, E., Moran-Zuloaga, D., Rizzo, L. V., 745 Rose, D., Su, H., Thalman, R., Walter, D., Wang, J., Wolff, S., Barbosa, H. M. J., Artaxo, P., Andreae, M. O., Pöschl, U., and Pöhlker, C.: Long-term observations of cloud condensation nuclei in the Amazon rain forest—Part 2: Variability and characteristic differences under



- near-pristine, biomass burning, and long-range transport conditions, *Atmos. Chem. Phys. Discuss.*, <https://doi.org/10.5194/acp-2017-847>, 2018.
- 750 Rafee, S. A. A., Martins, L. D., Kawashima, A. B., Almeida, D. S., Morais, M. V., Souza, R. V., Oliveira, M. B., Souza, R. A., Medeiros, A. S., Urbina, V., et al.: Contributions of mobile, stationary and biogenic sources to air pollution in the Amazon rainforest: a numerical study with the WRF-Chem model, *Atmos. Chem. Phys.*, 17, 7977, <https://doi.org/10.5194/acp-17-7977-2017>, 2017.
- Ramachandran, S. and Rajesh, T.: Black carbon aerosol mass concentrations over Ahmedabad, an urban location in western India: comparison with urban sites in Asia, Europe, Canada, and the United States, *J. Geophys. Res.-Atmos.*, 112, <https://doi.org/10.1029/2006JD007488>, 2007.
- 755 Rap, A., Spracklen, D., Mercado, L., Reddington, C., Haywood, J., Ellis, R., Phillips, O., Artaxo, P., Bonal, D., Restrepo Coupe, N., et al.: Fires increase Amazon forest productivity through increases in diffuse radiation, *Geophysical Research Letters*, 42, 4654–4662, <https://doi.org/10.1002/2015GL063719>, 2015.
- Rizzo, L. V., Correia, A. L., Artaxo, P., Procópio, A. S., and Andreae, M. O.: Spectral dependence of aerosol light absorption over the Amazon Basin, *Atmos. Chem. Phys.*, 11, 8899, <https://doi.org/10.5194/acp-11-8899-2011>, 2011.
- 760 Rizzo, L. V., Artaxo, P., Mueller, T., Wiedensohler, A., Paixao, M., Cirino, G. G., Arana, A., Swietlicki, E., Roldin, P., Fors, E. O., et al.: Long term measurements of aerosol optical properties at a primary forest site in Amazonia, <https://doi.org/10.5194/acp-13-2391-2013>, 2013.
- Rizzolo, J. A., Barbosa, C. G., Borillo, G. C., Godoi, A. F., Souza, R. A., Andreoli, R. V., Manzi, A. O., Sá, M. O., Alves, E. G., Pöhlker, C., et al.: Soluble iron nutrients in Saharan dust over the central Amazon rainforest, *Atmos. Chem. Phys.*, 17, 2673–2687, <https://doi.org/10.5194/acp-17-2673-2017>, 2017.
- 765 Romano, S., Perrone, M. R., Pavese, G., Esposito, F., and Calvello, M.: Optical properties of PM_{2.5} particles: Results from a monitoring campaign in southeastern Italy, *Atmos. Environ.*, 203, 35–47, <https://doi.org/10.1016/j.atmosenv.2019.01.037>, 2019.
- Russell, P., Bergstrom, R., Shinozuka, Y., Clarke, A., DeCarlo, P., Jimenez, J., Livingston, J., Redemann, J., Dubovik, O., and Strawa, A.: Absorption Angstrom Exponent in AERONET and related data as an indicator of aerosol composition, *Atmos. Chem. Phys.*, 10, 1155–1169, <https://doi.org/10.5194/acp-10-1155>, 2010.
- 770 Sánchez-Ccoyllo, O. R., Ynoue, R. Y., Martins, L. D., Astolfo, R., Miranda, R. M., Freitas, E. D., Borges, A. S., Fornaro, A., Freitas, H., Moreira, A., et al.: Vehicular particulate matter emissions in road tunnels in Sao Paulo, Brazil, *Environmental monitoring and assessment*, 149, 241–249, <https://doi.org/10.1007/s10661-008-0198-5>, 2009.
- Sarwar, G., Fahey, K., Napelenok, S., Roselle, S., and Mathur, R.: Examining the impact of CMAQ model updates on aerosol sulfate predictions, in: *The 10th Annual CMAS Models-3 User's Conference*, October, Chapel Hill, NC, 2011.
- 775 Saturno, J., Holanda, B. A., Pöhlker, C., Ditas, F., Wang, Q., Moran-Zuloaga, D., Brito, J., Carbone, S., Cheng, Y., Chi, X., et al.: Black and brown carbon over central Amazonia: Long-term aerosol measurements at the ATTO site, *Atmos. Chem. Phys.*, 18, 12 817–12 843, <https://doi.org/10.5194/acp-18-12817-2018>, 2018.
- Schultz, M. G., Schröder, S., Lyapina, O., Cooper, O. R., Galbally, I., Petropavlovskikh, I., Von Schneidmesser, E., Tanimoto, H., Elshorbany, Y., Naja, M., et al.: Tropospheric Ozone Assessment Report: Database and metrics data of global surface ozone observations, *Elementa: Science of the Anthropocene*, 5, <https://doi.org/10.1525/elementa.244>, 2017.
- 780 Seinfeld, J. H. and Pandis, S. N.: *Atmos. Chem. Phys.: from air pollution to climate change*, John Wiley & Sons, 2016.



- Shilling, J. E., Pekour, M. S., Fortner, E. C., Artaxo, P., Sá, S. d., Hubbe, J. M., Longo, K. M., Machado, L. A., Martin, S. T., Springston, S. R., et al.: Aircraft observations of the chemical composition and aging of aerosol in the Manaus urban plume during GoAmazon 2014/5, *Atmos. Chem. Phys.*, 18, 10 773–10 797, <https://doi.org/10.5194/acp-18-10773-2018>, 2018.
- 785 Shrivastava, M., Andreae, M. O., Artaxo, P., Barbosa, H. M., Berg, L. K., Brito, J., Ching, J., Easter, R. C., Fan, J., Fast, J. D., et al.: Urban pollution greatly enhances formation of natural aerosols over the Amazon rainforest, *Nature communications*, 10, 1–12, <https://doi.org/10.5194/acp-17-7977-2017>, 2019.
- Silva Dias, M. A. F., Silva Dias, P. L., Longo, M., Fitzjarrald, D. R., and Denning, A. S.: River breeze circulation in eastern Amazonia: observations and modelling results, *Theor. Appl. Climatol.*, 78, 111–121, <https://doi.org/10.1007/s00704-004-0047-6>, 2004.
- 790 Stein, A. F., Isakov, V., Godowitch, J., and Draxler, R. R.: A hybrid modeling approach to resolve pollutant concentrations in an urban area, *Atmos. Environ.*, 41, 9410–9426, <https://doi.org/10.1016/j.atmosenv.2007.09.004>, 2007.
- Tewari, M., Chen, F., Wang, W., Dudhia, J., LeMone, M., Mitchell, K., Ek, M., Gayno, G., Wegiel, J., and Cuenca, R.: Implementation and verification of the unified NOAA land surface model in the WRF model, in: 20th conference on weather analysis and forecasting/16th conference on numerical weather prediction, vol. 1115, pp. 2165–2170, American Meteorological Society Seattle, WA, 2004.
- 795 Trebs, I., Mayol-Bracero, O. L., Pauliquevis, T., Kuhn, U., Sander, R., Ganzeveld, L., Meixner, F. X., Kesselmeier, J., Artaxo, P., and Andreae, M. O.: Impact of the Manaus urban plume on trace gas mixing ratios near the surface in the Amazon Basin: Implications for the NO-NO₂-O₃ photostationary state and peroxy radical levels, *J. Geophys. Res.-Atmos.*, 117, <https://doi.org/10.1029/2011JD016386>, 2012.
- 800 Vara-Vela, A., de Fátima Andrade, M., Zhang, Y., Kumar, P., Ynoue, R. Y., Souto-Oliveira, C. E., da Silva Lopes, F. J., and Landulfo, E.: Modeling of Atmospheric Aerosol Properties in the São Paulo Metropolitan Area: Impact of Biomass Burning, *J. Geophys. Res.-Atmos.*, 123, 9935–9956, <https://doi.org/10.1029/2018JD028768>, 2018.
- Wang, K., Zhang, Y., Yahya, K., Wu, S.-Y., and Grell, G.: Implementation and initial application of new chemistry-aerosol options in WRF/Chem for simulating secondary organic aerosols and aerosol indirect effects for regional air quality, *Atmos. Environ.*, 115, 716–732, 2015.
- 805 Yáñez-Serrano, A. M., Bourtsoukidis, E., Alves, E. G., Bauwens, M., Stavrou, T., Llusà, J., Filella, I., Guenther, A., Williams, J., Artaxo, P., et al.: Amazonian biogenic volatile organic compounds under global change, *Global Change Biology*, <https://doi.org/10.1111/gcb.15185>, 2020.
- Ynoue, R. Y. and Andrade, M. F.: Size-resolved mass balance of aerosol particles over the São Paulo metropolitan area of Brazil, *Aerosol Science and Technology*, 38, 52–62, 2004.
- 810 Zhang, Y., Wen, X.-Y., and Jang, C.: Simulating chemistry–aerosol–cloud–radiation–climate feedbacks over the continental US using the online-coupled Weather Research Forecasting Model with chemistry (WRF/Chem), *Atmos. Environ.*, 44, 3568–3582, 2010.